Generalizations of the Kerr-Newman solution

Contents

1 Topics

- Generalizations of the Kerr-Newman solution
- Properties of Kerr-Newman spacetimes
- Quadrupolar metrics

1.1 ICRANet Participants

- Roy P. Kerr
- Hernando Quevedo
- Jorge A. Rueda
- Remo Ruffini

1.2 Ongoing collaborations

- Medeu Abishev (Kazakh National University - KazNU, Kazakhstan)
- Nurzada Beissen (Taraz State Pedagogical University, Kazakhstan)
- Kuantay Boshkayev (Kazakh National University - KazNU, Kazakhstan)
- Antonio C. Gutierrez (Industrial University of Santander, Colombia)
- Orlando Luongo (University of Naples, Italy)
- Daniela Pugliese (Silesian University in Opava, Czech Republic)
- Saken Toktarbay (Kazakh National University - KazNU, Kazakhstan)

1.3 Students

- Jesús Anaya, (UNAM, PhD, Mexico)
- Fernando Aragón (UNAM PhD, Mexico)
- Aizhan Mansurova (KazNU PhD, Kazakhstan)
- Walter Pulido (Universidad Nacional de Colombia)
- Luis M. Sánchez (UNAM PhD, Mexico)
- Pedro Sánchez (UNAM PhD, Mexico)
- Servando Vargas (UNAM PhD, Mexico)
- Sasha Zaldivar (UNAM PhD, Mexico)

2 Brief description

One of the most important metrics in general relativity is the Kerr-Newman solution that describes the gravitational and electromagnetic fields of a rotating charged mass. For astrophysical purposes, however, it is necessary to take into account the effects due to the moment of inertia of the object. To attack this problem, we investigate new exact solutions of Einstein-Maxwell equations which posses an infinite set of gravitational and electromagnetic multipole moments and contain the Kerr-Newman solution as special case.

In particular, we derive an approximate solution of Einstein equations, describing the gravitational field of a mass distribution that slightly deviates from spherical symmetry. The deviation is described by means of a quadrupole parameter that is responsible for the appearance of a curvature singularity, which is not covered by a horizon of the limiting Schwarzschild spacetime. We investigate the motion of test particles in the gravitational field of this naked singularity and show that the quadrupole parameter affects the properties of Schwarzschild trajectories. By investigating radial geodesics, we find that no effects of repulsive gravity are present. We interpreted this result as indicating that repulsive gravity is a non-linear effect, which manifests itself only on certain test particle trajectories.

An important problem for investigating the physical meaning of solutions of Einstein's equations is the matching problem, which consists in matching together two spacetimes. In this context, we apply the Darmois and the C^3 matching conditions to three different spherically symmetric spacetimes. The exterior spacetime is described by the Schwarzschild vacuum solution whereas for the interior counterpart we choose different perfect fluid solutions with the same symmetry. We show that Darmois matching conditions are satisfied in all the three cases whereas the C^3 conditions are not fulfilled. We argue that this difference is due to a non-physical behavior of the pressure on the matching surface.

The behavior of matter in the gravitational field of a compact object described by a solution of Einstein's equations is important to explore the physical meaning of mathematical solutions. In this framework, we investigate the luminosity of the accretion disk for a static black hole surrounded by dark matter with anisotropic pressure. We calculate all basic orbital parameters of test particles in the accretion disk, such as

angular velocity, angular momentum, energy and radius of the innermost circular stable orbit as functions of the dark matter density, radial pressure and anisotropic parameter, which establishes the relationship between the radial and tangential pressures. We show that the presence of dark matter with anisotropic pressure makes a noticeable difference in the geometry around a Schwarzschild black hole, affecting the radiative flux, differential luminosity and spectral luminosity of the accretion disk.

3 Introduction

It is hard to overemphasize the importance of the Kerr geometry not only for general relativity itself, but also for the very fundamentals of physics. It assumes this position as being the most physically relevant rotating generalization of the static Schwarzschild geometry. Its charged counterpart, the Kerr-Newman solution, representing the exterior gravitational and electromagnetic fields of a charged rotating object, is an exact solution of the Einstein-Maxwell equations.

Its line element in Boyer–Lindquist coordinates can be written as

$$\begin{aligned} ds^2 &= \frac{r^2 - 2Mr + a^2 + Q^2}{r^2 + a^2\cos^2\theta}(dt - a\sin^2\theta d\varphi)^2 \\ &\quad - \frac{\sin^2\theta}{r^2 + a^2\cos^2\theta}[(r^2 + a^2)d\varphi - adt]^2 \\ &\quad - \frac{r^2 + a^2\cos^2\theta}{r^2 - 2Mr + a^2 + Q^2}dr^2 - (r^2 + a^2\cos^2\theta)d\theta^2 \,, \end{aligned} \tag{3.0.1}$$

where M is the total mass of the object, $a = J/M$ is the specific angular momentum, and Q is the electric charge. In this particular coordinate system, the metric functions do not depend on the coordinates t and ϕ, indicating the existence of two Killing vector fields $\xi^I = \partial_t$ and $\xi^{II} = \partial_\varphi$ which represent the properties of stationarity and axial symmetry, respectively.

An important characteristic of this solution is that the source of gravity is surrounded by two horizons situated at a distance

$$r_\pm = M \pm \sqrt{M^2 - a^2 - Q^2} \tag{3.0.2}$$

from the origin of coordinates. Inside the interior horizon, r_-, a ring singularity is present which, however, cannot be observed by any observer situated outside the exterior horizon. If the condition $M^2 < a^2 + Q^2$ is satisfied, no horizons are present and the Kerr–Newman spacetime represents the exterior field of a naked singularity.

Despite of its fundamental importance in general relativity, and its theoretical and mathematical interest, this solution has not been especially useful for describing as-

trophysical phenomena, first of all, because observed astrophysical objects do not possess an appreciable net electric charge. Furthermore, the limiting Kerr metric takes into account the mass and the rotation, but does not consider the moment of inertia of the object. For astrophysical applications it is, therefore, necessary to use more general solutions with higher multipole moments which are due not only to the rotation of the body but also to its shape. This means that even in the limiting case of a static spacetime, a solution is needed that takes into account possible deviations from spherically symmetry.

4 The general static vacuum solution

In general relativity, stationary axisymmetric solutions of Einstein's equations [45] play a crucial role for the description of the gravitational field of astrophysical objects. In particular, the black hole solutions and their generalizations that include Maxwell fields are contained within this class.

This type of exact solutions has been the subject of intensive research during the past few decades. In particular, the number of know exact solutions drastically increased after Ernst [11] discovered an elegant representation of the field equations that made it possible to search for their symmetries. These studies lead finally to the development of solution generating techniques [45] which allow us to find new solutions, starting from a given seed solution. In particular, solutions with an arbitrary number of multipole moments for the mass and angular momentum were derived in [44] and used to describe the gravitational field of rotating axially symmetric distributions of mass.

The first analysis of stationary axially symmetric gravitational fields was carried out by Weyl [48] in 1917, soon after the formulation of general relativity. In particular, Weyl discovered that in the static limit the main part of the vacuum field equations reduces to a single linear differential equation. The corresponding general solution can be written in cylindrical coordinates as an infinite sum with arbitrary constant coefficients. A particular choice of the coefficients leads to the subset of asymptotically flat solutions which is the most interesting from a physical point of view. In this section we review the main properties of stationary axisymmetric gravitational fields. In particular, we show explicitly that the main field equations in vacuum can be represented as the equations of a nonlinear sigma model in which the base space is the 4-dimensional spacetime and the target space is a 2-dimensional conformally Euclidean space.

4.1 Line element and field equations

Although there exist in the literature many suitable coordinate systems, stationary axisymmetric gravitational fields are usually described in cylindric coordinates (t, ρ, z, φ).

Stationarity implies that t can be chosen as the time coordinate and the metric does not depend on time, i.e. $\partial g_{\mu\nu}/\partial t = 0$. Consequently, the corresponding timelike Killing vector has the components δ^{μ}_{t}. A second Killing vector field is associated to the axial symmetry with respect to the axis $\rho = 0$. Then, choosing φ as the azimuthal angle, the metric satisfies the conditions $\partial g_{\mu\nu}/\partial\varphi = 0$, and the components of the corresponding spacelike Killing vector are δ^{μ}_{φ}.

Using further the properties of stationarity and axial symmetry, together with the vacuum field equations, for a general metric of the form $g_{\mu\nu} = g_{\mu\nu}(\rho, z)$, it is possible to show that the most general line element for this type of gravitational fields can be written in the Weyl-Lewis-Papapetrou form as [48, 26, 36]

$$ds^2 = f(dt - \omega d\varphi)^2 - f^{-1}\left[e^{2\gamma}(d\rho^2 + dz^2) + \rho^2 d\varphi^2\right] , \tag{4.1.1}$$

where f, ω and γ are functions of ρ and z, only. After some rearrangements which include the introduction of a new function $\Omega = \Omega(\rho, z)$ by means of

$$\rho\partial_\rho\Omega = f^2\partial_z\omega , \qquad \rho\partial_z\Omega = -f^2\partial_\rho\omega , \tag{4.1.2}$$

the vacuum field equations $R_{\mu\nu} = 0$ can be shown to be equivalent to the following set of partial differential equations

$$\frac{1}{\rho}\partial_\rho(\rho\partial_\rho f) + \partial_z^2 f + \frac{1}{f}[(\partial_\rho\Omega)^2 + (\partial_z\Omega)^2 - (\partial_\rho f)^2 - (\partial_z f)^2] = 0 , \tag{4.1.3}$$

$$\frac{1}{\rho}\partial_\rho(\rho\partial_\rho\Omega) + \partial_z^2\Omega - \frac{2}{f}\left(\partial_\rho f\,\partial_\rho\Omega + \partial_z f\,\partial_z\Omega\right) = 0 , \tag{4.1.4}$$

$$\partial_\rho\gamma = \frac{\rho}{4f^2}\left[(\partial_\rho f)^2 + (\partial_\rho\Omega)^2 - (\partial_z f)^2 - (\partial_z\Omega)^2\right] , \tag{4.1.5}$$

$$\partial_z\gamma = \frac{\rho}{2f^2}\left(\partial_\rho f\,\partial_z f + \partial_\rho\Omega\,\partial_z\Omega\right) . \tag{4.1.6}$$

It is clear that the field equations for γ can be integrated by quadratures, once f and Ω are known. For this reason, the equations (4.1.3) and (4.1.4) for f and Ω are usually considered as the main field equations for stationary axisymmetric vacuum gravitational fields. In the following subsections we will focus on the analysis of the main field equations, only. It is interesting to mention that this set of equations can be geometrically interpreted in the context of nonlinear sigma models [19].

Let us consider the special case of static axisymmetric fields. This corresponds to

metrics which, apart from being axially symmetric and independent of the time coordinate, are invariant with respect to the transformation $\varphi \to -\varphi$ (i.e. rotations with respect to the axis of symmetry are not allowed). Consequently, the corresponding line element is given by (4.1.1) with $\omega = 0$, and the field equations can be written as

$$\partial_\rho^2 \psi + \frac{1}{\rho}\partial_\rho \psi + \partial_z^2 \psi = 0 \,, \quad f = \exp(2\psi) \,, \tag{4.1.7}$$

$$\partial_\rho \gamma = \rho \left[(\partial_\rho \psi)^2 - (\partial_z \psi)^2 \right] \,, \quad \partial_z \gamma = 2\rho \partial_\rho \psi \, \partial_z \psi \,. \tag{4.1.8}$$

We see that the main field equation (4.1.7) corresponds to the linear Laplace equation for the metric function ψ.

4.2 Static solution

The general solution of Laplace's equation is known and, if we demand additionally asymptotic flatness, we obtain the Weyl solution which can be written as [48, 45]

$$\psi = \sum_{n=0}^{\infty} \frac{a_n}{(\rho^2 + z^2)^{\frac{n+1}{2}}} P_n(\cos\theta) \,, \qquad \cos\theta = \frac{z}{\sqrt{\rho^2 + z^2}} \,, \tag{4.2.1}$$

where a_n $(n = 0, 1, ...)$ are arbitrary constants, and $P_n(\cos\theta)$ represents the Legendre polynomials of degree n. The expression for the metric function γ can be calculated by quadratures by using the set of first order differential equations (4.1.8). Then

$$\gamma = -\sum_{n,m=0}^{\infty} \frac{a_n a_m (n+1)(m+1)}{(n+m+2)(\rho^2 + z^2)^{\frac{n+m+2}{2}}} \left(P_n P_m - P_{n+1} P_{m+1} \right) \,. \tag{4.2.2}$$

Since this is the most general static, axisymmetric, asymptotically flat vacuum solution, it must contain all known solution of this class. In particular, one of the most interesting special solutions which is Schwarzschild's spherically symmetric black hole spacetime must be contained in this class. To see this, we must choose the constants a_n in such a way that the infinite sum (4.2.1) converges to the Schwarzschild solution in cylindric coordinates. But, or course, this representation is not the most appropriate to analyze the interesting physical properties of Schwarzschild's metric.

In fact, it turns out that to investigate the properties of solutions with multipole moments it is more convenient to use prolate spheroidal coordinates (t, x, y, φ) in

which the line element can be written as

$$ds^2 = f dt^2 - \frac{\sigma^2}{f}\left[e^{2\gamma}(x^2-y^2)\left(\frac{dx^2}{x^2-1}+\frac{dy^2}{1-y^2}\right)+(x^2-1)(1-y^2)d\varphi^2\right]$$

where

$$x = \frac{r_+ + r_-}{2\sigma}\,, \quad (x^2 \geq 1), \quad y = \frac{r_+ - r_-}{2\sigma}\,, \quad (y^2 \leq 1) \tag{4.2.3}$$

$$r_\pm^2 = \rho^2 + (z \pm \sigma)^2\,, \quad \sigma = const\,, \tag{4.2.4}$$

and the metric functions are f, ω, and γ depend on x and y, only. In this coordinate system, the general static solution which is also asymptotically flat can be expressed as

$$f = \exp(2\psi)\,, \quad \psi = \sum_{n=0}^{\infty}(-1)^{n+1} q_n P_n(y) Q_n(x)\,, \quad q_n = const$$

where $P_n(y)$ are the Legendre polynomials, and $Q_n(x)$ are the Legendre functions of second kind. In particular,

$$P_0 = 1, \quad P_1 = y, \quad P_2 = \frac{1}{2}(3y^2-1)\,, ...$$

$$Q_0 = \frac{1}{2}\ln\frac{x+1}{x-1}\,, \quad Q_1 = \frac{1}{2}x\ln\frac{x+1}{x-1} - 1\,,$$
$$Q_2 = \frac{1}{2}(3x^2-1)\ln\frac{x+1}{x-1} - \frac{3}{2}x\,, ...$$

The corresponding function γ can be calculated by quadratures and its general expression has been explicitly derived in [40]. The most important special cases contained in this general solution are the Schwarzschild metric

$$\psi = -q_0 P_0(y) Q_0(x)\,, \quad \gamma = \frac{1}{2}\ln\frac{x^2-1}{x^2-y^2}\,,$$

and the Erez-Rosen metric [10]

$$\psi = -q_0 P_0(y) Q_0(x) - q_2 P_2(y) Q_2(x)\,, \quad \gamma = \frac{1}{2}\ln\frac{x^2-1}{x^2-y^2} + ...$$

In the last case, the constant parameter q_2 turns out to determine the quadrupole moment. In general, the constants q_n represent an infinite set of parameters that de-

termines an infinite set of mass multipole moments. The parameters q_n represent the deviation of the mass distribution from the ideal spherical symmetry. It is interesting to mention that if demand the additional symmetry with respect to the equatorial plane $\theta = \pi/2$, it can be shown that all odd parameters q_{2k+1}, $k = 0, 1, ...$ should vanish. This is an additional symmetry condition that reduces the form of the resulting metric.

5 Stationary generalization

The solution generating techniques [22] can be applied, in particular, to any static seed solution in order to obtain the corresponding stationary generalization. One of the most powerful techniques is the inverse method (ISM) developed by Belinski and Zakharov [49]. We used a particular case of the ISM, which is known as the Hoenselaers–Kinnersley-Xanthopoulos (HKX) transformation to derive the stationary generalization of the general static solution in prolate spheroidal coordinates.

5.1 Ernst representation

In the general stationary case ($\omega \neq 0$) with line element

$$\begin{aligned} & ds^2 = f(dt - \omega d\varphi)^2 \\ - \quad & \frac{\sigma^2}{f}\left[e^{2\gamma}(x^2-y^2)\left(\frac{dx^2}{x^2-1}+\frac{dy^2}{1-y^2}\right)+(x^2-1)(1-y^2)d\varphi^2\right] \end{aligned}$$

it is useful to introduce the the Ernst potentials

$$E = f + i\Omega\,, \quad \xi = \frac{1-E}{1+E}\,,$$

where the function Ω is now determined by the equations

$$\sigma(x^2-1)\Omega_x = f^2\omega_y\,, \quad \sigma(1-y^2)\Omega_y = -f^2\omega_x\,.$$

Then, the main field equations can be represented in a compact and symmetric form:

$$(\xi\xi^*-1)\left\{[(x^2-1)\xi_x]_x + [(1-y^2)\xi_y]_y\right\} = 2\xi^*[(x^2-1)\xi_x^2 + (1-y^2)\xi_y^2]\,.$$

This equation is invariant with respect to the transformation $x \leftrightarrow y$. Then, since the particular solution

$$\xi = \frac{1}{x} \rightarrow \Omega = 0 \rightarrow \omega = 0 \rightarrow \gamma = \frac{1}{2} \ln \frac{x^2 - 1}{x^2 - y^2}$$

represents the Schwarzschild spacetime, the choice $\xi^{-1} = y$ is also an exact solution. Furthermore, if we take the linear combination $\xi^{-1} = c_1 x + c_2 y$ and introduce it into the field equation, we obtain the new solution

$$\xi^{-1} = \frac{\sigma}{M} x + i \frac{a}{M} y \, , \; \sigma = \sqrt{M^2 - a^2} \, ,$$

which corresponds to the Kerr metric in prolate spheroidal coordinates.

In the case of the Einstein-Maxwell theory, the main field equations can be expressed as

$$(\xi\xi^* - \mathcal{F}\mathcal{F}^* - 1)\nabla^2 \xi = 2(\xi^* \nabla \xi - \mathcal{F}^* \nabla \mathcal{F}) \nabla \xi \, ,$$
$$(\xi\xi^* - \mathcal{F}\mathcal{F}^* - 1)\nabla^2 \mathcal{F} = 2(\xi^* \nabla \xi - \mathcal{F}^* \nabla \mathcal{F}) \nabla \mathcal{F}$$

where ∇ represents the gradient operator in prolate spheroidal coordinates. Moreover, the gravitational potential ξ and the electromagnetic $\mathcal{F}$ Ernst potential are defined as

$$\xi = \frac{1 - f - i\Omega}{1 + f + i\Omega} \, , \quad \mathcal{F} = 2 \frac{\Phi}{1 + f + i\Omega} \, .$$

The potential Φ can be shown to be determined uniquely by the electromagnetic potentials A_t and A_φ One can show that if ξ_0 is a vacuum solution, then the new potential

$$\xi = \xi_0 \sqrt{1 - e^2}$$

represents a solution of the Einstein-Maxwell equations with effective electric charge e. This transformation is known in the literature as the Harrison transformation [18]. Accordingly, the Kerr–Newman solution in this representation acquires the simple form

$$\xi = \frac{\sqrt{1 - e^2}}{\frac{\sigma}{M} x + i \frac{a}{M} y} \, , \qquad e = \frac{Q}{M} \, , \qquad \sigma = \sqrt{M^2 - a^2 - Q^2} \, .$$

In this way, it is very easy to generalize any vacuum solution to include the case of electric charge. More general transformations of this type can be used in order to generate solutions with any desired set of gravitational and electromagnetic multipole moments [41].

5.2 Representation as a nonlinear sigma model

Consider two (pseudo)-Riemannian manifolds (M, γ) and (N, G) of dimension m and n, respectively. Let M be coordinatized by x^a, and N by X^μ, so that the metrics on M and N can be, in general, smooth functions of the corresponding coordinates, i.e., $\gamma = \gamma(x)$ and $G = G(X)$. A harmonic map is a smooth map $X : M \to N$, or in coordinates $X : x \longmapsto X$ so that X becomes a function of x, and the X's satisfy the motion equations following from the action [33]

$$S = \int d^m x \sqrt{|\gamma|}\, \gamma^{ab}(x)\, \partial_a X^\mu\, \partial_b X^\nu\, G_{\mu\nu}(X)\,, \tag{5.2.1}$$

which sometimes is called the "energy" of the harmonic map X. The straightforward variation of S with respect to X^μ leads to the motion equations

$$\frac{1}{\sqrt{|\gamma|}} \partial_b \left(\sqrt{|\gamma|} \gamma^{ab} \partial_a X^\mu \right) + \Gamma^\mu_{\ \nu\lambda}\, \gamma^{ab}\, \partial_a X^\nu\, \partial_b X^\lambda = 0\,, \tag{5.2.2}$$

where $\Gamma^\mu_{\ \nu\lambda}$ are the Christoffel symbols associated to the metric $G_{\mu\nu}$ of the target space N. If $G_{\mu\nu}$ is a flat metric, one can choose Cartesian-like coordinates such that $G_{\mu\nu} = \eta_{\mu\nu} = diag(\pm 1, ..., \pm 1)$, the motion equations become linear, and the corresponding sigma model is linear. This is exactly the case of a bosonic string on a flat background in which the base space is the 2-dimensional string world-sheet. In this case the action (5.2.1) is usually referred to as the Polyakov action [37].

Consider now the case in which the base space M is a stationary axisymmetric spacetime. Then, γ^{ab}, $a, b = 0, ..., 3$, can be chosen as the Weyl-Lewis-Papapetrou metric (4.1.1), i.e.

$$\gamma_{ab} = \begin{pmatrix} f & 0 & 0 & -f\omega \\ 0 & -f^{-1}e^{2k} & 0 & 0 \\ 0 & 0 & -f^{-1}e^{2k} & 0 \\ -f\omega & 0 & 0 & f\omega^2 - \rho^2 f^{-1} \end{pmatrix}. \tag{5.2.3}$$

Let the target space N be 2-dimensional with metric $G_{\mu\nu} = (1/2) f^{-2} \delta_{\mu\nu}$, $\mu, \nu = 1, 2$, and let the coordinates on N be $X^\mu = (f, \Omega)$. Then, it is straightforward to show that the action (5.2.1) becomes

$$S = \int \mathcal{L}\, dt d\varphi d\rho dz\,, \qquad \mathcal{L} = \frac{\rho}{2f^2} \left[(\partial_\rho f)^2 + (\partial_z f)^2 + (\partial_\rho \Omega)^2 + (\partial_z \Omega)^2 \right]\,, \tag{5.2.4}$$

and the corresponding motion equations (5.2.2) are identical to the main field equations (4.1.3) and (4.1.4).

Notice that the field equations can also be obtained from (5.2.4) by a direct variation with respect to f and Ω. This interesting result was obtained originally by Ernst [11], and is the starting point of what today is known as the Ernst representation of the field equations.

The above result shows that stationary axisymmetric gravitational fields can be described as a $(4 \to 2)-$nonlinear harmonic map, where the base space is the spacetime of the gravitational field and the target space corresponds to a 2-dimensional conformally Euclidean space. A further analysis of the target space shows that it can be interpreted as the quotient space $SL(2,R)/SO(2)$, and the Lagrangian (5.2.4) can be written explicitly [6] in terms of the generators of the Lie group $SL(2,R)$. Harmonic maps in which the target space is a quotient space are usually known as nonlinear sigma models [33].

The form of the Lagrangian (5.2.4) with two gravitational field variables, f and Ω, depending on two coordinates, ρ and z, suggests a representation as a harmonic map with a 2-dimensional base space. In string theory, this is an important fact that allows one to use the conformal invariance of the base space metric to find an adequate representation for the set of classical solutions. This, in turn, facilitates the application of the canonical quantization procedure. Unfortunately, this is not possible for the Lagrangian (5.2.4). Indeed, if we consider γ^{ab} as a 2-dimensional metric that depends on the parameters ρ and z, the diagonal form of the Lagrangian (5.2.4) implies that $\sqrt{|\gamma|}\gamma^{ab} = \delta^{ab}$. Clearly, this choice is not compatible with the factor ρ in front of the Lagrangian. Therefore, the reduced gravitational Lagrangian (5.2.4) cannot be interpreted as corresponding to a $(2 \to n)$-harmonic map. Nevertheless, we will show in the next section that a modification of the definition of harmonic maps allows us to "absorb" the unpleasant factor ρ in the metric of the target space, and to use all the advantages of a 2-dimensional base space.

Notice that the representation of stationary fields as a nonlinear sigma model becomes degenerate in the limiting case of static fields. Indeed, the underlying geometric structure of the $SL(2,R)/SO(2)$ nonlinear sigma models requires that the target space be 2-dimensional, a condition which is not satisfied by static fields. We will see below that by using a dimensional extension of generalized sigma models, it will be possible to treat the special static case, without affecting the underlying geometric structure.

The analysis performed in this section for stationary axisymmetric fields can be generalized to include any gravitational field containing two commuting Killing vec-

tor fields [45]. This is due to the fact that for this class of gravitational fields it is always possible to find the corresponding Ernst representation in which the Lagrangian contains only two gravitational variables which depend on only two spacetime coordinates.

5.3 Representation as a generalized harmonic map

Consider two (pseudo-)Riemannian manifolds (M, γ) and (N, G) of dimension m and n, respectively. Let x^a and X^μ be coordinates on M and N, respectively. This coordinatization implies that in general the metrics γ and G become functions of the corresponding coordinates. Let us assume that not only γ but also G can explicitly depend on the coordinates x^a, i.e. let $\gamma = \gamma(x)$ and $G = G(X, x)$. This simple assumption is the main aspect of our generalization which, as we will see, lead to new and nontrivial results.

A smooth map $X : M \to N$ will be called an $(m \to n)-$generalized harmonic map if it satisfies the Euler-Lagrange equations

$$\frac{1}{\sqrt{|\gamma|}}\partial_b\left(\sqrt{|\gamma|}\gamma^{ab}\partial_a X^\mu\right) + \Gamma^\mu_{\ \nu\lambda}\,\gamma^{ab}\,\partial_a X^\nu \partial_b X^\lambda + G^{\mu\lambda}\gamma^{ab}\,\partial_a X^\nu\,\partial_b G_{\lambda\nu} = 0\,, \qquad (5.3.1)$$

which follow from the variation of the generalized action

$$S = \int d^m x \sqrt{|\gamma|}\,\gamma^{ab}(x)\,\partial_a\,X^\mu \partial_b X^\nu G_{\mu\nu}(X, x)\,, \qquad (5.3.2)$$

with respect to the fields X^μ. Here the Christoffel symbols, determined by the metric $G_{\mu\nu}$, are calculated in the standard manner, without considering the explicit dependence on x. Notice that the new ingredient in this generalized definition of harmonic maps, i.e., the term $G_{\mu\nu}(X, x)$ in the Lagrangian density implies that we are taking into account the "interaction" between the base space M and the target space N. This interaction leads to an extra term in the motion equations, as can be seen in (5.3.1). It turns out that this interaction is the result of the effective presence of the gravitational field.

Notice that the limiting case of generalized linear harmonic maps is much more complicated than in the standard case. Indeed, for the motion equations (5.3.1) to become linear it is necessary that the conditions

$$\gamma^{ab}(\Gamma^\mu_{\ \nu\lambda}\,\partial_b X^\lambda + G^{\mu\lambda}\,\partial_b G_{\lambda\nu})\partial_a X^\nu = 0\,, \qquad (5.3.3)$$

be satisfied. One could search for a solution in which each term vanishes separately. The choice of a (pseudo-)Euclidean target metric $G_{\mu\nu} = \eta_{\mu\nu}$, which would imply $\Gamma^{\mu}_{\ \nu\lambda} = 0$, is not allowed, because it would contradict the assumption $\partial_b G_{\mu\nu} \neq 0$. Nevertheless, a flat background metric in curvilinear coordinates could be chosen such that the assumption $G^{\mu\lambda}\partial_b G_{\mu\nu} = 0$ is fulfilled, but in this case $\Gamma^{\mu}_{\ \nu\lambda} \neq 0$ and (5.3.3) cannot be satisfied. In the general case of a curved target metric, conditions (5.3.3) represent a system of m first order nonlinear partial differential equations for $G_{\mu\nu}$. Solutions to this system would represent linear generalized harmonic maps. The complexity of this system suggests that this special type of maps is not common.

As we mentioned before, the generalized action (5.3.2) includes an interaction between the base space N and the target space M, reflected on the fact that $G_{\mu\nu}$ depends explicitly on the coordinates of the base space. Clearly, this interaction must affect the conservation laws of the physical systems we attempt to describe by means of generalized harmonic maps. To see this explicitly we calculate the covariant derivative of the generalized Lagrangian density

$$\mathcal{L} = \sqrt{|\gamma|}\,\gamma^{ab}(x)\,\partial_a X^{\mu}\partial_b X^{\nu} G_{\mu\nu}(X,x)\,, \tag{5.3.4}$$

and replace in the result the corresponding motion equations (5.3.1). Then, the final result can be written as

$$\nabla_b \widetilde{T}_a^{\ b} = -\frac{\partial \mathcal{L}}{\partial x^a} \tag{5.3.5}$$

where $\widetilde{T}_a^{\ b}$ represents the canonical energy-momentum tensor

$$\widetilde{T}_a^{\ b} = \frac{\partial \mathcal{L}}{\partial(\partial_b X^{\mu})}(\partial_a X^{\mu}) - \delta_a^b \mathcal{L} = 2\sqrt{\gamma} G_{\mu\nu}\left(\gamma^{bc}\partial_a X^{\mu}\,\partial_c X^{\nu} - \frac{1}{2}\delta_a^b \gamma^{cd}\partial_c X^{\mu}\,\partial_d X^{\nu}\right). \tag{5.3.6}$$

The standard conservation law is recovered only when the Lagrangian does not depend explicitly on the coordinates of the base space. Even if we choose a flat base space $\gamma_{ab} = \eta_{ab}$, the explicit dependence of the metric of the target space $G_{\mu\nu}(X,x)$ on x generates a term that violates the standard conservation law. This term is due to the interaction between the base space and the target space which, consequently, is one of the main characteristics of the generalized harmonic maps introduced in this work.

An alternative and more general definition of the energy-momentum tensor is by means of the variation of the Lagrangian density with respect to the metric of the base

space, i.e.

$$T_{ab} = \frac{\delta \mathcal{L}}{\delta \gamma^{ab}} \,. \tag{5.3.7}$$

A straightforward computation shows that for the action under consideration here we have that $\widetilde{T}_{ab} = 2T_{ab}$ so that the generalized conservation law (5.3.5) can be written as

$$\nabla_b T_a{}^b + \frac{1}{2}\frac{\partial \mathcal{L}}{\partial x^a} = 0 \,. \tag{5.3.8}$$

For a given metric on the base space, this represents in general a system of m differential equations for the "fields" X^μ which must be satisfied "on-shell".

If the base space is 2-dimensional, we can use a reparametrization of x to choose a conformally flat metric, and the invariance of the Lagrangian density under arbitrary Weyl transformations to show that the energy-momentum tensor is traceless, $T_a{}^a = 0$.

In Section 5.1 we described stationary, axially symmetric, gravitational fields as a $(4 \to 2)-$nonlinear sigma model. There it was pointed out the convenience of having a 2-dimensional base space in analogy with string theory. Now we will show that this can be done by using the generalized harmonic maps defined above.

Consider a $(2 \to 2)-$generalized harmonic map. Let $x^a = (\rho, z)$ be the coordinates on the base space M, and $X^\mu = (f, \Omega)$ the coordinates on the target space N. In the base space we choose a flat metric and in the target space a conformally flat metric, i.e.

$$\gamma_{ab} = \delta_{ab} \qquad \text{and} \qquad G_{\mu\nu} = \frac{\rho}{2f^2}\delta_{\mu\nu} \qquad (a, b = 1, 2;\ \mu, \nu = 1, 2). \tag{5.3.9}$$

A straightforward computation shows that the generalized Lagrangian (5.3.4) coincides with the Lagrangian (5.2.4) for stationary axisymetric fields, and that the equations of motion (5.3.1) generate the main field equations (4.1.3) and (4.1.4).

For the sake of completeness we calculate the components of the energy-momentum tensor $T_{ab} = \delta\mathcal{L}/\delta\gamma^{ab}$. Then

$$T_{\rho\rho} = -T_{zz} = \frac{\rho}{4f^2}\left[(\partial_\rho f)^2 + (\partial_\rho \Omega)^2 - (\partial_z f)^2 - (\partial_z \Omega)^2\right], \tag{5.3.10}$$

$$T_{\rho z} = \frac{\rho}{2f^2}\left(\partial_\rho f\, \partial_z f + \partial_\rho \Omega\, \partial_z \Omega\right). \tag{5.3.11}$$

This tensor is traceless due to the fact that the base space is 2-dimensional. It satisfies

the generalized conservation law (5.3.8) on-shell:

$$\frac{dT_{\rho\rho}}{d\rho} + \frac{dT_{\rho z}}{dz} + \frac{1}{2}\frac{\partial \mathcal{L}}{\partial \rho} = 0 \,, \tag{5.3.12}$$

$$\frac{dT_{\rho z}}{d\rho} - \frac{dT_{\rho\rho}}{dz} = 0 \,. \tag{5.3.13}$$

Incidentally, the last equation coincides with the integrability condition for the metric function k, which is identically satisfied by virtue of the main field equations. In fact, as can be seen from Eqs.(4.1.5,4.1.6) and (5.3.10,5.3.11), the components of the energy-momentum tensor satisfy the relationships $T_{\rho\rho} = \partial_\rho k$ and $T_{\rho z} = \partial_z k$, so that the conservation law (5.3.13) becomes an identity. Although we have eliminated from the starting Lagrangian (5.2.4) the variable k by applying a Legendre transformation on the Einstein-Hilbert Lagrangian (see [6] for details) for this type of gravitational fields, the formalism of generalized harmonic maps seems to retain the information about k at the level of the generalized conservation law.

The above results show that stationary axisymmetric spacetimes can be represented as a $(2 \to 2)-$generalized harmonic map with metrics given as in (5.3.9). It is also possible to interpret the generalized harmonic map given above as a generalized string model. Although the metric of the base space M is Euclidean, we can apply a Wick rotation $\tau = i\rho$ to obtain a Minkowski-like structure on M. Then, M represents the world-sheet of a bosonic string in which τ is measures the time and z is the parameter along the string. The string is "embedded" in the target space N whose metric is conformally flat and explicitly depends on the time parameter τ. We will see in the next section that this embedding becomes more plausible when the target space is subject to a dimensional extension. In the present example, it is necessary to apply a Wick rotation in order to interpret the base space as a string world-sheet. This is due to the fact that both coordinates ρ and z are spatial coordinates. However, this can be avoided by considering other classes of gravitational fields with timelike Killing vector fields; examples will be given below.

The most studied solutions belonging to the class of stationary axisymmetric fields are the asymptotically flat solutions. Asymptotic flatness imposes conditions on the metric functions which in the cylindrical coordinates used here can be formulated in the form

$$\lim_{x^a\to\infty} f = 1 + O\left(\frac{1}{x^a}\right) \,, \quad \lim_{x^a\to\infty} \omega = c_1 + O\left(\frac{1}{x^a}\right) \,, \quad \lim_{x^a\to\infty} \Omega = O\left(\frac{1}{x^a}\right) \tag{5.3.14}$$

where c_1 is an arbitrary real constant which can be set to zero by appropriately choosing the angular coordinate φ. If we choose the domain of the spatial coordinates as $\rho \in [0, \infty)$ and $z \in (-\infty, +\infty)$, from the asymptotic flatness conditions it follows that the coordinates of the target space N satisfy the boundary conditions

$$\dot{X}^{\mu}(\rho, -\infty) = 0 = \dot{X}^{\mu}(\rho, \infty) \,, \quad X'^{\mu}(\rho, -\infty) = 0 = X'^{\mu}(\rho, \infty) \tag{5.3.15}$$

where the dot stands for a derivative with respect to ρ and the prime represents derivation with respect to z. These relationships are known in string theory [37] as the Dirichlet and Neumann boundary conditions for open strings, respectively, with the extreme points situated at infinity. We thus conclude that if we assume ρ as a "time" parameter for stationary axisymmetric gravitational fields, an asymptotically flat solution corresponds to an open string with endpoints attached to $D-$branes situated at plus and minus infinity in the $z-$direction.

5.4 Dimensional extension

In order to further analyze the analogy between gravitational fields and bosonic string models, we perform an arbitrary dimensional extension of the target space N, and study the conditions under which this dimensional extension does not affect the field equations of the gravitational field. Consider an $(m \to D)-$generalized harmonic map. As before we denote by $\{x^a\}$ the coordinates on M. Let $\{X^{\mu}, X^{\alpha}\}$ with $\mu = 1, 2$ and $\alpha = 3, 4, ..., D$ be the coordinates on N. The metric structure on M is again $\gamma = \gamma(x)$, whereas the metric on N can in general depend on all coordinates of M and N, i.e. $G = G(X^{\mu}, X^{\alpha}, x^a)$. The general structure of the corresponding field equations is as given in (5.3.1). They can be divided into one set of equations for X^{μ} and one set of equations for X^{α}. According to the results of the last section, the class of gravitational fields under consideration can be represented as a $(2 \to 2)-$generalized harmonic map so that we can assume that the main gravitational variables are contained in the coordinates X^{μ} of the target space. Then, the gravitational sector of the target space will be contained in the components $G_{\mu\nu}$ $(\mu, \nu = 1, 2)$ of the metric, whereas the components $G_{\alpha\beta}$ $(\alpha, \beta = 3, 4, ..., D)$ represent the sector of the dimensional extension.

Clearly, the set of differential equations for X^{μ} also contains the variables X^{α} and its derivatives $\partial_a X^{\alpha}$. For the gravitational field equations to remain unaffected by this dimensional extension we demand the vanishing of all the terms containing X^{α} and its derivatives in the equations for X^{μ}. It is easy to show that this can be achieved by

imposing the conditions

$$G_{\mu\alpha} = 0\,, \quad \frac{\partial G_{\mu\nu}}{\partial X^{\alpha}} = 0\,, \quad \frac{\partial G_{\alpha\beta}}{\partial X^{\mu}} = 0\,. \tag{5.4.1}$$

That is to say that the gravitational sector must remain completely invariant under a dimensional extension, and the additional sector cannot depend on the gravitational variables, i.e., $G_{\alpha\beta} = G_{\alpha\beta}(X^{\gamma}, x^{a})$, $\gamma = 3, 4, ..., D$. Furthermore, the variables X^{α} must satisfy the differential equations

$$\frac{1}{\sqrt{|\gamma|}}\partial_b\left(\sqrt{|\gamma|}\gamma^{ab}\partial_a X^{\alpha}\right) + \Gamma^{\alpha}_{\ \beta\gamma}\,\gamma^{ab}\,\partial_a X^{\beta}\partial_b X^{\gamma} + G^{\alpha\beta}\gamma^{ab}\,\partial_a X^{\gamma}\,\partial_b G_{\beta\gamma} = 0\,. \tag{5.4.2}$$

This shows that any given $(2 \to 2)-$generalized map can be extended, without affecting the field equations, to a $(2 \to D)-$generalized harmonic map.

It is worth mentioning that the fact that the target space N becomes split in two separate parts implies that the energy-momentum tensor $T_{ab} = \delta\mathcal{L}/\delta\gamma^{ab}$ separates into one part belonging to the gravitational sector and a second one following from the dimensional extension, i.e. $T_{ab} = T_{ab}(X^{\mu}, x) + T_{ab}(X^{\alpha}, x)$. The generalized conservation law as given in (5.3.8) is satisfied by the sum of both parts.

Consider the example of stationary axisymmetric fields given the metrics (5.3.9). Taking into account the conditions (5.4.1), after a dimensional extension the metric of the target space becomes

$$G = \begin{pmatrix} \frac{\rho}{2f^2} & 0 & 0 & \cdots & 0 \\ 0 & \frac{\rho}{2f^2} & 0 & \cdots & 0 \\ 0 & 0 & G_{33}(X^{\alpha}, x) & \cdots & G_{3D}(X^{\alpha}, x) \\ . & . & \cdots & \cdots & \cdots \\ 0 & 0 & G_{D3}(X^{\alpha}, x) & \cdots & G_{DD}(X^{\alpha}, x) \end{pmatrix}. \tag{5.4.3}$$

Clearly, to avoid that this metric becomes degenerate we must demand that $\det(G_{\alpha\beta}) \neq 0$, a condition that can be satisfied in view of the arbitrariness of the components of the metric. With the extended metric, the Lagrangian density gets an additional term

$$\begin{aligned} \mathcal{L} = \quad & \frac{\rho}{2f^2}\left[(\partial_\rho f)^2 + (\partial_z f)^2 + (\partial_\rho \Omega)^2 + (\partial_z \Omega)^2\right] \\ & + \left(\partial_\rho X^{\alpha}\partial_\rho X^{\beta} + \partial_z X^{\alpha}\partial_z X^{\beta}\right) G_{\alpha\beta}\,, \end{aligned} \tag{5.4.4}$$

which nevertheless does not affect the field equations for the gravitational variables f and Ω. On the other hand, the new fields must be solutions of the extra field equations

$$\left(\partial_\rho^2 + \partial_z^2\right) X^\alpha + \Gamma^\alpha{}_{\beta\gamma}\left(\partial_\rho X^\beta \partial_\rho X^\gamma + \partial_z X^\beta \partial_z X^\gamma\right) \tag{5.4.5}$$

$$+G^{\alpha\gamma}\left(\partial_\rho X^\beta \partial_\rho G_{\beta\gamma} + \partial_z X^\beta \partial_z G_{\beta\gamma}\right) = 0\,. \tag{5.4.6}$$

An interesting special case of the dimensional extension is the one in which the extended sector is Minkowskian, i.e. for the choice $G_{\alpha\beta} = \eta_{\alpha\beta}$ with additional fields X^α given as arbitrary harmonic functions. This choice opens the possibility of introducing a "time" coordinate as one of the additional dimensions, an issue that could be helpful when dealing with the interpretation of gravitational fields in this new representation.

The dimensional extension finds an interesting application in the case of static axisymmetric gravitational fields. As mentioned in Section 4.1, these fields are obtained from the general stationary fields in the limiting case $\Omega = 0$ (or equivalently, $\omega = 0$). If we consider the representation as an $SL(2,R)/SO(2)$ nonlinear sigma model or as a $(2 \to 2)-$generalized harmonic map, we see immediately that the limit $\Omega = 0$ is not allowed because the target space becomes 1-dimensional and the underlying metric is undefined. To avoid this degeneracy, we first apply a dimensional extension and only then calculate the limiting case $\Omega = 0$. In the most simple case of an extension with $G_{\alpha\beta} = \delta_{\alpha\beta}$, the resulting $(2 \to 2)-$generalized map is described by the metrics $\gamma_{ab} = \delta_{ab}$ and

$$G = \begin{pmatrix} \frac{\rho}{2f^2} & 0 \\ 0 & 1 \end{pmatrix} \tag{5.4.7}$$

where the additional dimension is coordinatized by an arbitrary harmonic function which does not affect the field equations of the only remaining gravitational variable f. This scheme represents an alternative method for exploring static fields on nondegenerate target spaces. Clearly, this scheme can be applied to the case of gravitational fields possessing two hypersurface orthogonal Killing vector fields.

Our results show that a stationary axisymmetric field can be represented as a string "living" in a D-dimensional target space N. The string world-sheet is parametrized by the coordinates ρ and z. The gravitational sector of the target space depends explicitly on the metric functions f and Ω and on the parameter ρ of the string world-sheet. The sector corresponding to the dimensional extension can be chosen as a $(D-2)-$dimensional Minkowski spacetime with time parameter τ. Then, the string world-sheet is a 2-dimensional flat hypersurface which is "frozen" along the time τ.

5.5 The general solution

If we take as seed metric the general static solution, the application of two HXK transformations generates a stationary solution with an infinite number of gravitoelectric and gravitomagnetic multipole moments. The HKX method is applied at the level of the Ernst potential from which the metric functions can be calculated by using the definition of the Ernst potential E and the field equations for γ. The resulting expressions in the general case are quite cumbersome. We quote here only the special case in which only an arbitrary quadrupole parameter is present. In this case, the result can be written as

$$\begin{aligned} f &= \frac{R}{L} e^{-2qP_2Q_2} , \\ \omega &= -2a - 2\sigma \frac{\mathcal{M}}{R} e^{2qP_2Q_2} , \\ e^{2\gamma} &= \frac{1}{4}\left(1+\frac{M}{\sigma}\right)^2 \frac{R}{x^2-y^2} e^{2\hat{\gamma}} , \end{aligned} \tag{5.5.1}$$

where

$$\begin{aligned} R &= a_+a_- + b_+b_- , \qquad L = a_+^2 + b_+^2 , \\ \mathcal{M} &= \alpha x(1-y^2)(e^{2q\delta_+} + e^{2q\delta_-})a_+ + y(x^2-1)(1-\alpha^2 e^{2q(\delta_+ + \delta_-)})b_+ , \\ \hat{\gamma} &= \frac{1}{2}(1+q)^2 \ln\frac{x^2-1}{x^2-y^2} + 2q(1-P_2)Q_1 + q^2(1-P_2)\Big[(1+P_2)(Q_1^2-Q_2^2) \\ &\quad + \frac{1}{2}(x^2-1)(2Q_2^2 - 3xQ_1Q_2 + 3Q_0Q_2 - Q_2')\Big] . \end{aligned} \tag{5.5.2}$$

Here $P_l(y)$ and $Q_l(x)$ are Legendre polynomials of the first and second kind respectively. Furthermore

$$\begin{aligned} a_\pm &= x(1-\alpha^2 e^{2q(\delta_+ + \delta_-)}) \pm (1+\alpha^2 e^{2q(\delta_+ + \delta_-)}) , \\ b_\pm &= \alpha y(e^{2q\delta_+} + e^{2q\delta_-}) \mp \alpha(e^{2q\delta_+} - e^{2q\delta_-}) , \\ \delta_\pm &= \frac{1}{2}\ln\frac{(x\pm y)^2}{x^2-1} + \frac{3}{2}(1-y^2 \mp xy) + \frac{3}{4}[x(1-y^2) \mp y(x^2-1)]\ln\frac{x-1}{x+1} , \end{aligned}$$

the quantity α being a constant

$$\alpha = \frac{\sigma - M}{a}\,, \qquad \sigma = \sqrt{M^2 - a^2}\,. \tag{5.5.3}$$

The physical significance of the parameters entering this metric can be clarified by calculating the Geroch-Hansen [13, 17] multipole moments

$$M_{2k+1} = J_{2k} = 0\,, \quad k = 0, 1, 2, ... \tag{5.5.4}$$

$$M_0 = M\,, \quad M_2 = -Ma^2 + \frac{2}{15}qM^3\left(1 - \frac{a^2}{M^2}\right)^{3/2}\,, ... \tag{5.5.5}$$

$$J_1 = Ma\,, \quad J_3 = -Ma^3 + \frac{4}{15}qM^3a\left(1 - \frac{a^2}{M^2}\right)^{3/2}\,, ... \tag{5.5.6}$$

The vanishing of the odd gravitoelectric (M_n) and even gravitomagnetic (J_n) multipole moments is a consequence of the symmetry with respect to the equatorial plane. From the above expressions we see that M is the total mass of the body, a represents the specific angular momentum, and q is related to the deviation from spherical symmetry. All higher multipole moments can be shown to depend only on the parameters M, a, and q.

We analyzed the geometric and physical properties of the above solution. The special cases contained in the general solution suggest that it can be used to describe the exterior asymptotically flat gravitational field of rotating body with arbitrary quadrupole moment. This is confirmed by the analysis of the motion of particles on the equatorial plane. The quadrupole moment turns out to drastically change the geometric structure of spacetime as well as the motion of particles, especially near the gravitational source.

We investigated in detail the properties of the Quevedo-Mashhoon (QM) spacetime which is a generalization of Kerr spacetime, including an arbitrary quadrupole. Our results show [4] that a deviation from spherical symmetry, corresponding to a nonzero electric quadrupole, completely changes the structure of spacetime. A similar behavior has been found in the case of the Erez-Rosen spacetime. In fact, a naked singularity appears that affects the ergosphere and introduces regions where closed timelike curves are allowed. Whereas in the Kerr spacetime the ergosphere corresponds to the boundary of a simply-connected region of spacetime, in the present case the ergosphere is distorted by the presence of the quadrupole and can even become transformed into non simply-connected regions. All these changes occur near

the naked singularity which is situated at $x = 1$, a value that corresponds to the radial distance $r = M + \sqrt{M^2 - a^2}$ in Boyer-Lindquist coordinates. In the limiting case $a/M > 1$, the multipole moments and the metric become complex, indicating that the physical description breaks down. Consequently, the extreme Kerr black hole represents the limit of applicability of the QM spacetime.

Since standard astrophysical objects satisfy the condition $a/M < 1$, we can conclude that the QM metric can be used to describe their exterior gravitational field. Two alternative situations are possible. If the characteristic radius of the body is greater than the critical distance $M + \sqrt{M^2 - a^2}$, i.e. $x > 1$, the exterior solution must be matched with an interior solution in order to describe the entire spacetime. If, however, the characteristic radius of the body is smaller than the critical distance $M + \sqrt{M^2 - a^2}$, the QM metric describes the field of a naked singularity.

6 Gravitational field of slightly deformed naked singularities

6.1 Introduction

Although the existence of naked singularities in Nature is the subject of intense debate nowadays, it has been well established that Einstein field equations for the gravitational field allow solutions that can be interpreted as describing naked singularities. In particular, black hole solutions are characterized by the existence of naked singularity counterparts [24]. However, it seems that the particular choice of the physical parameters, which is necessary for the formation of naked singularities, is difficult to be realizable in Nature. Indeed, a rotating naked singularity needs a specific angular momentum that must be greater that its mass (in geometric units), a condition that probably cannot be fulfilled in realistic configurations because it would imply such a high angular velocity that the object would destroy itself before reaching it [34].

There is, however, a simpler way to generate naked singularities, namely, by considering mass distributions with quadrupole moment [42]. Indeed, from the point of view of multipole moments, the uniqueness theorems prove that black holes can have only mass monopole and angular momentum dipole [21]. Consequently, the addition of a quadrupole to a mass distribution, even in the static case, would imply that the corresponding gravitational field describes a naked singularity. Consequently, a simple shape deviation from spherical symmetry in a mass distribution leads to the appearance of naked singularities. In previous works [42**? ?** , 5], we used a particular static quadrupolar solution [50, 47, 32, 45] to study the physical properties of naked singularities.

There are several solutions of Einstein field equations that can be used to describe the exterior gravitational field of a static mass distribution with quadrupole moment [12]. In the limiting case of vanishing quadrupole, they reduce to the spacetime of a Schwarzschild black hole. An interesting characteristic of all of them is that the outermost naked singularity is a sphere with radius $r = 2m$, where m is the mass of the gravitational source. This could be interpreted intuitively as if the presence of the

quadrupole causes the destruction of the regular horizon turning it into a singular hypersurface.

In this work, we show that this is not always the case. Indeed, we will derive a new solution, whose singularity is located on a sphere of radius $r = m$. This means that in this case the quadrupole completely destroys the regular horizon at $r = 2m$, but generates a new special hypersurface at $r = m$ which contains a singularity. To derive this new solution, we use the fact in realistic situations we expect that compact objects deviates only slightly from spherical symmetry. This implies that the quadrupole can be considered as a small quantity. With this in mind, we investigate a particular approximate line element, which is valid only up to the first order in the quadrupole parameter. Then, we find the general solution of the corresponding Einstein vacuum field equations and show that a particular solution is characterized by a curvature singularity located on a sphere of radius $r = m$.

This work is organized as follows. In Sec. 6.2, we consider a line element that is especially adapted to the study of interior and exterior solutions. We derive the general field equations for the case of vacuum gravitational fields. In Sec. 6.3, we find the most general solution that is linear in the quadrupole moment. We select a particular case that is characterized by the presence of naked singularity at a distance $r = m$ from the origin of coordinates. We also calculate the Newtonian limit of the new approximate solution and show that it corresponds to a mass distribution with a small quadrupole. In Sec. 6.4, we investigate the motion of test particles in the spacetime described by the approximate solution. In general, we find that the quadrupole affects the behavior of Schwarzschild orbits. By analyzing the behavior of free falling particles we show that no effects associated with the presence of repulsive gravity can be detected in contrast to repulsive effects found previously in the case of exact solutions with quadrupole. We conclude that repulsive gravity in naked singularities is a non-linear phenomenon. Finally, Sec. 7.6 contains a summary of our results.

6.2 Line element and field equations

The search for and investigation of physically meaningful solutions of Einstein equations begins with the choice of an appropriate line element. In the case of static gravitational fields of deformed mass distributions, one can assume that the fields preserve axial symmetry. Moreover, if we are interested in describing the gravitational field outside as well as inside the mass distribution, it is convenient to choose a line element that can be used in both cases. In a previous work [1], we found interior perfect-fluid solutions that can be matched with exterior vacuum solutions under the

assumption that the quadrupole moment is small. From a physical point of view, this implies that the mass distribution is only slightly deformed. We were able to find a particular line element that can be used to search for interior and exterior approximate solutions. It can be written as

$$\begin{aligned} ds^2 = \quad & e^{2\nu}(1+qa)dt^2 - (1+qc+qb)\frac{dr^2}{1-\frac{2\tilde{m}}{r}} \\ & -(1+qa+qb)r^2 d\theta^2 - (1-qa)r^2\sin^2\theta d\varphi^2 \,, \end{aligned} \tag{6.2.1}$$

where the set of (t, r, θ, φ) can be interpreted as polar coordinates in the limiting case $q \to 0$. Moreover, the functions $\nu = \nu(r)$, $a = a(r)$, $c = c(r)$, $\tilde{m} = \tilde{m}(r)$, and $b = b(r, \theta)$ are arbitrary.

In the particular case $q = 0$, the above line element can be used to describe the exterior Schwarzschild solution

$$\tilde{m} = m = const,\ e^{2\nu} = 1 - \frac{2m}{r} \,, \tag{6.2.2}$$

and the interior perfect fluid Schwarzschild metric with

$$\tilde{m} = 4\pi\rho R^3 \,,\ p = \frac{3m}{4\pi R^3}\frac{[f(r) - f(R)]}{[3f(R) - f(r)]} \,, \tag{6.2.3}$$

with

$$e^{2\nu} = \left[\frac{3}{2}f\left(R\right) - \frac{1}{2}f\left(r\right)\right]^2,\ f\left(r\right) = \sqrt{1 - \frac{2mr^2}{R^3}} \tag{6.2.4}$$

where $\rho = const$ and $p = p(r)$ are the density and pressure of the fluid, respectively.

Furthermore, for $q \neq 0$ the line element (6.2.1) contains the approximate (up to the first order in q) quadrupolar metric ($q-$metric), which has been interpreted as the simplest generalization of the Schwarzschild metric that includes a quadrupole moment [42]. In this limit, q has been interpreted as the quadrupole parameter.

Here, we will use the advantages of the line element (6.2.1) to search for more general approximate solutions. Then, the Einstein vacuum field equations, up to the first order in q, can be written as

$$\tilde{m}_{,r} = 0 \quad i.e. \quad \tilde{m} = m = const. \,, \tag{6.2.5}$$

$$\nu_{,r} = \frac{m}{r\left(r - 2m\right)} \,, \tag{6.2.6}$$

$$(r-m)(a_{,r}-c_{,r})+(a-c)=0\,, \tag{6.2.7}$$

$$\begin{aligned} 2 \quad & r\,(r-2m)\,a_{,rr}+(3r-m)\,a_{,r}+(r-3m)\,c_{,r} \\ & -2\,(a-c)=0, \end{aligned} \tag{6.2.8}$$

$$\begin{aligned} r \quad & (r-2m)\,b_{,rr}+b_{,\theta\theta}+(r-m)\,b_{,r}-2\,(r-2m)\,c_{,r} \\ & +2\,(a-c)=0, \end{aligned} \tag{6.2.9}$$

$$\begin{aligned} & \left(r^2-2mr+m^2\sin^2\theta\right)b_{,\theta}+2r\,(r-2m) \\ & \times\,(ma_{,r}-a+c)\sin\theta\cos\theta=0, \end{aligned} \tag{6.2.10}$$

$$\begin{aligned} & \left(r^2-2mr+m^2\sin^2\theta\right)b_{,r}+2\,(r-2m) \\ & \times\left(r-m\sin^2\theta\right)a_{,r}+2\,(r-m)\,(a-c)\sin^2\theta=0, \end{aligned} \tag{6.2.11}$$

where a comma represents partial differentiation with respect to the corresponding coordinate. For simplicity, we replaced the solution of the first equation $\tilde{m}=m=const.$ in the remaining equations.

6.3 Approximate solutions

We now investigate the system of partial differential equation (6.2.6)-(6.2.11). Equations (6.2.6) and (6.2.7) can be integrated and yield

$$\nu=\frac{1}{2}\ln\left(1-\frac{2m}{r}\right)+\alpha_1\,,\quad a-c=\frac{\alpha_2 m^2}{(r-m)^2}\,, \tag{6.3.1}$$

where α_1 and α_2 are dimensionless integration constants. It turns out that the remaining system of partial differential equations can be integrated in general and yields

$$a=-\frac{\alpha_2 m}{r-m}+\frac{1}{2}\,(\alpha_3-\alpha_2)\ln\left(1-\frac{2m}{r}\right)+\alpha_4\,, \tag{6.3.2}$$

$$c = -\frac{\alpha_2 mr}{(r-m)^2} + \frac{1}{2}(\alpha_3 - \alpha_2)\ln\left(1 - \frac{2m}{r}\right) + \alpha_4\,, \tag{6.3.3}$$

$$\begin{aligned} b = \;& \frac{2\alpha_2 m}{r-m} - (\alpha_3 - \alpha_2)\left[\ln 2\right. \\ + \;& \left.\ln\left(1 - \frac{2m}{r} + \frac{m^2\sin^2\theta}{r^2}\right)\right] + \alpha_5\,, \end{aligned} \tag{6.3.4}$$

where α_3, α_4, and α_5 are dimensionless integration constants. We can see that the general approximate exterior solution with quadrupole moment is represented by the 5-parameter family of solutions (6.3.1)–(6.3.4). In this general solution, the additive constants α_4 and α_5 can be chosen such that at infinity the solution describes the Minkowski spacetime in spherical coordinates. This means that non asymptotically flat solutions are also contained in the above general solution.

To partially investigate the physical meaning of this solution, we calculate the Kretschmann scalar $K = R_{abcd}R^{abcd}$. We obtain

$$\begin{aligned} K = \;& \frac{48m^2}{r^6}\left\{1 + q\left[(\alpha_2 - \alpha_3)\left[\ln\left(1 - \frac{2m}{r}\right)\right.\right.\right. \\ - \;& \left.2\ln\left(1 - \frac{2m}{r} + \frac{m^2}{r^2}\sin^2\theta\right) - 2\ln 2\right] \\ +\alpha_2 \;& \left.\left.A_1 + \alpha_3 A_2 - 2(\alpha_4 + \alpha_5) + \alpha_2 A_3\right] + \mathcal{O}(q^2)\right\} \end{aligned} \tag{6.3.5}$$

where

$$\begin{aligned} A_1 \;=\; & -\frac{1}{6\left(m^2\sin^2\theta - 2mr + r^2\right)(m-r)^3 m^2} \\ \times \;& \left[\left(12m^3 - 11m^2 r - 14mr^2 + 11r^3\right)m^4\cos^2\theta\right. \\ - \;& \left.\left(12m^3 - 17m^2 r - 2mr^2 + 5r^3\right)m^2(m-r)^2\right] \end{aligned} \tag{6.3.6}$$

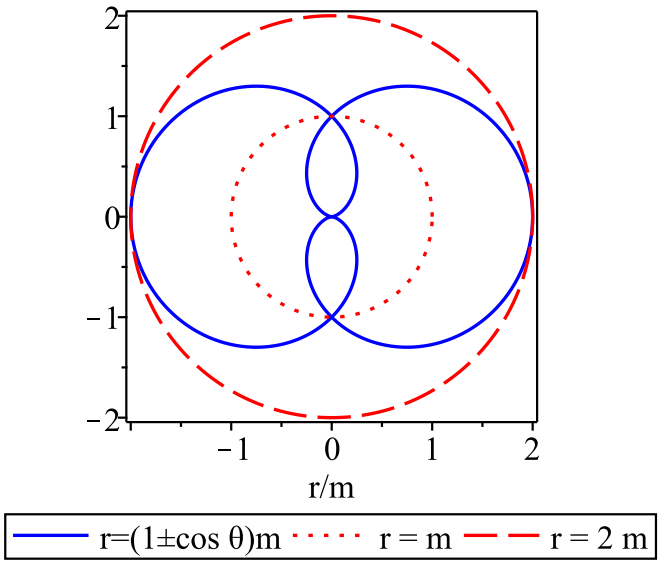

Figure 6.1: Curvature singularities of the general metric.

$$A_2 = \frac{2m^2 \sin^2\theta - 3mr + r^2}{m^2 \sin^2\theta - 2mr + r^2} \tag{6.3.7}$$

$$A_3 = -\frac{1}{6}\frac{r\left[7\,(m-r)^2 - 2r^2\right]}{(m-r)^3} \tag{6.3.8}$$

where the term proportional to q^2 has been neglected. We can see that this approximate spacetime is characterized by the presence of three different curvature singularities located at

$$r = 0\,, \quad r = m \quad r = 2m\,, \quad r = m(1 \pm \cos\theta)\,. \tag{6.3.9}$$

The geometric structure of the curvature singularities of the solutions (6.3.1), (6.3.2), (6.3.3) and (6.3.4) is illustrated in Fig.6.1.

Another interesting particular case corresponds to the choice

$$\alpha_1 = 0\,, \quad \alpha_3 = \alpha_2\,, \quad \alpha_4 = 0\,, \quad \alpha_5 = 0\,, \tag{6.3.10}$$

which leads to the line element

$$\begin{aligned} ds^2 &= \left(1-\frac{2m}{r}\right)\left(1-\frac{q\alpha_2 m}{r-m}\right)dt^2 \\ &\quad -\left[1+\frac{q\alpha_2 m(r-2m)}{(r-m)^2}\right]\frac{dr^2}{1-\frac{2m}{r}} \\ &\quad -\left(1+\frac{q\alpha_2 m}{r-m}\right)r^2(d\theta^2+\sin^2\theta d\varphi^2)\,. \end{aligned} \tag{6.3.11}$$

This is an asymptotically flat approximate solution with parameters m, q and α_2. Since α_2 appears always in combination with q, it can be absorbed in the definition of q. We, therefore, set $\alpha_2 = 1$ without loss of generality. The singularity structure can be found by analyzing the Kretschmann invariant, which in this case reduces to

$$K = \frac{48m^2}{r^6}\left(1+q\frac{r-4m}{r-m}+\mathcal{O}(q^2)\right)\,. \tag{6.3.12}$$

We see that there are only two singularities, which are located at $r = 0$ and $r = m$. This is an interesting property of this solution because all the remaining solutions contained in (6.3.1)–(6.3.4) are singular on the hypersurface $r = 2m$. Moreover, all the known exact solutions with quadrupole turn out to be singular at $r = 2m$ [12]. To our knowledge, the solution (6.3.11) is the only one in which the outermost singularity is located inside the sphere with $r = 2m$. This means that the spacetime is well defined behind in the interval $r \in (m, 2m]$. We are interested in investigating the properties of this spacetime near the singularity $r = m$.

To further analyze the physical meaning of the solution (6.3.11), we calculate the corresponding Newtonian limit. To this end, we perform a coordinate transformation of the form $(r, \theta) \to (R, \vartheta)$ defined by the equations [1, 2]

$$\begin{aligned} r &= R\Bigg[1-q\frac{m}{R}\Big[1+\frac{m}{R}\left(\beta_1+\sin^2\vartheta\right) \\ &\quad + \frac{m^2}{R^2}\left(\beta_2-\sin^2\vartheta\right)+..\Big]\sin^2\vartheta\Bigg], \end{aligned} \tag{6.3.13}$$

and

$$\theta = \vartheta - q\frac{m^2}{R^2}\left(1+2\frac{m}{R}+...\right)\sin\vartheta\cos\vartheta, \tag{6.3.14}$$

where the β_1 and β_2 are constants and we have neglected terms of the order higher that m^3/R^3. Inserting the above coordinates into the metric (6.3.11), we obtain the approximate line element

$$\begin{aligned} ds^2 &= (1+2\Phi)\,dt^2 - \frac{dR^2}{1+2\Phi} \\ &- U(R,\vartheta)\,R^2\left(d\vartheta^2 + \sin^2\vartheta d\varphi^2\right), \end{aligned} \tag{6.3.15}$$

with

$$\Phi = -\frac{GM}{R} + \frac{GQ}{R^3}P_2(\cos\vartheta), \tag{6.3.16}$$

$$U(R,\vartheta) = 1 - 2\frac{GM}{R^3}P_2(\cos\vartheta), \tag{6.3.17}$$

where $P_2(\cos\vartheta)$ is the Legendre polynomial of degree 2, and we have chosen the free constants as $\alpha_2 = 2$, $\beta_1 = 1/3$, and $\beta_2 = 5/3$.

We recognize the metric (6.3.15) as the Newtonian limit of general relativity, where Φ represents the Newtonian potential. Moreover, the constants

$$M = (1+q)\,m, \quad Q = \frac{2}{3}qm^3, \tag{6.3.18}$$

can be interpreted as the Newtonian mass and quadrupole moment of the corresponding mass distribution.

6.4 Motion of test particles

Consider the trajectory $x^a(\tau)$ of a test particle with 4-velocity $u^a = dx^a/d\tau = \dot{x}^a$. The 4-moment $p^a = \mu\dot{x}^a$ of the particle can be normalized so that the equations and constraint for geodesics are given as

$$\ddot{x}^a + \Gamma^a{}_{bc}\dot{x}^b\dot{x}^c = 0 \tag{6.4.1}$$

$$g_{ab}\dot{x}^a\dot{x}^b = \epsilon, \tag{6.4.2}$$

where $\epsilon = 0, 1, -1$ for null, timelike, and spacelike curves, respectively [38]. For the approximate metric (6.3.11) we obtain from (6.4.1) that geodesics are determined, in

general, by the following set of equations

$$\ddot{t} + m\left[\frac{2}{r\,(r-2m)} + \frac{q}{(r-m)^2}\right]\dot{t}\dot{r} = 0\,, \tag{6.4.3}$$

$$\begin{aligned}
&\ddot{r} + \left[1 + \frac{q\left(6m^2 - 6mr + r^2\right)}{2\,(r-m)^2}\right]\frac{m\,(r-2m)\,\dot{t}^2}{r^3} \\
&-\frac{m}{2}\left[\frac{2}{r\,(r-2m)} + \frac{q\,(r-3m)}{(r-m)^3}\right]\dot{r}^2 \\
&-\left[r - 2m - \frac{qm\,(r-2m)^2}{(r-m)^2}\right]\dot{\theta}^2 \\
&-(r-2m)\sin^2\theta\left[1 - \frac{qm\,(r-2m)}{(r-m)^2}\right]\dot{\varphi}^2 = 0\,,
\end{aligned} \tag{6.4.4}$$

$$\ddot{\theta} - \sin\theta\cos\theta\dot{\varphi}^2 + \left(\frac{2}{r} - \frac{qm}{(r-m)^2}\right)\dot{r}\dot{\theta} = 0. \tag{6.4.5}$$

$$\ddot{\varphi} + \left[\left(\frac{2}{r} - \frac{qm}{(r-m)^2}\right)\dot{r} + \frac{2\cos\theta}{\sin\theta}\dot{\theta}\right]\dot{\varphi} = 0\,, \tag{6.4.6}$$

The 4-moment $p^a = \mu\dot{x}^a$ of the particle can be normalized so that

$$g_{ab}\dot{x}^a\dot{x}^b = \epsilon, \tag{6.4.7}$$

where $\epsilon = 0, 1, -1$ for null, timelike, and spacelike curves, respectively [39]. Then, for the approximate metric (6.3.11) we obtain from (6.4.7) that

$$\left(1 - \frac{qm^2}{(r-m)}\right)\dot{r}^2 = \tilde{E}^2 - \Phi^2, \tag{6.4.8}$$

where

$$V_{eff} = \Phi^2 = \left(1-\frac{2m}{r}\right)\left[r^2\dot{\theta}^2+\left(\epsilon+\frac{2l^2}{r^2\sin^2\theta}\right)\times\left(1-\frac{qm}{r-m}\right)-\frac{l^2}{r^2\sin^2\theta}\right] \tag{6.4.9}$$

is the effective potential and we have used the expression for the energy $E=\mu\tilde{E}$ and the angular moment $l=\mu\tilde{l}$ of the test particle which are constants of motion

$$E = g_{ab}\xi^a_t p^b = \left(1-\frac{2m}{r}\right)\left(1-\frac{qm}{r-m}\right)\mu\dot{t}, \tag{6.4.10}$$

$$l = -g_{ab}\xi^a_\varphi p^b = \left(1+\frac{qm}{r-m}\right)r^2\sin^2\theta\mu\dot{\varphi}, \tag{6.4.11}$$

associated with the Killing vector fields $\xi_t=\partial_t$ and $\xi_\varphi=\partial_\varphi$, respectively. For the sake of simplicity we set $\mu=1$ so that $\tilde{E}=E$ and $\tilde{l}=l$.

Figure 6.2 illustrates the behavior of the effective potential in terms of the parameter q for $\theta=\pi/2$. The effective potential of the Schwarzschild spacetime is also shown for comparison. For positive (negative) values of q, the effective potential at a given point outside the outer singularity is always less (greater) than the Schwarzschild value. This indicates that the distribution of orbits on the equator of the metric (6.2.1) can depend drastically on the value of q.

6.4.1 Circular orbits

We will now investigate the properties of circular orbits on the equatorial plane, $\theta=\pi/2$ of the gravitational described by the approximate metric (6.2.1). Circular orbits correspond to the limiting case $\dot{r}=0$. Their stability properties are determined by the extrema of the effective potential. Following the conventional stability analysis of

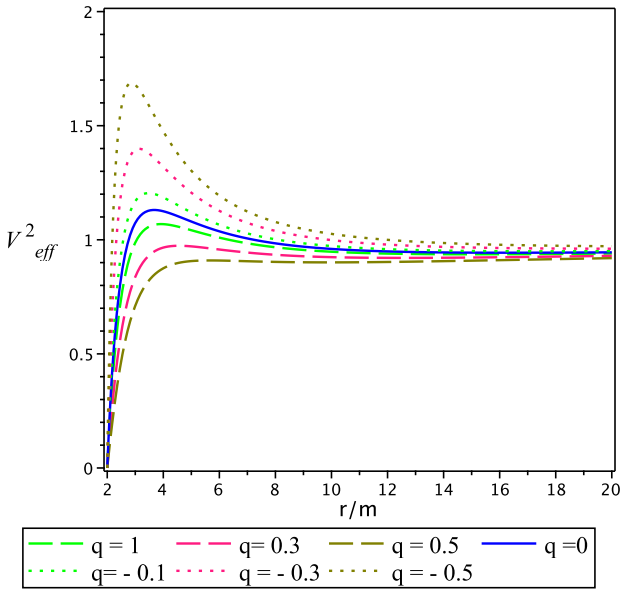

Figure 6.2: The effective potential for timelike geodesics on the equatorial plane as a function of the radius for different values of the quadrupole parameter. Here we set $l^2 = 20$ for concreteness.

circular orbits involving a potential function, from Eq.(6.4.9), we obtain

$$\begin{aligned} V_{eff,r} = & \frac{2\epsilon m}{r^2} + \frac{2\left(3m - r\right) l^2}{r^4} + \frac{qm}{r^2\left(r-m\right)^2} \\ \times & \left[\left(2m^2 - 4mr + r^2\right)\epsilon \right. \\ + & \left. \frac{2\left(6m^2 - 10mr + 3r^2\right) l^2}{r^2}\right], \end{aligned} \tag{6.4.12}$$

and

$$V_{eff,rr} = B_1 + B_2 \tag{6.4.13}$$

where B_1 and B_2 are given by

$$B_1 = \frac{m\left(36m^4 - 90m^3 r + 74m^2 r^2 - 22mr^3 + 2r^4\right)}{r^3\left(3m^2 - 4mr + r^2\right)^2}, \tag{6.4.14}$$

$$B_2 = \frac{mq\left(36m^4 - 114m^3 r + 74m^2 r^2 - 17mr^3 + r^4\right)}{r^3\left(3m^2 - 4mr + r^2\right)^2} \tag{6.4.15}$$

where we set $\epsilon = 1$ and replaced the value of the angular momentum

$$\begin{aligned} l^2 = & \frac{\epsilon m r^2}{\left(r-m\right)\left(r-3m\right)^2}\left[2\left(3m^2 - 4mr + r^2\right)\right. \\ + & \left. q\left(r^2 - 6m^2\right)\right], \end{aligned} \tag{6.4.16}$$

which can be derived from the condition $V_{eff,r} = 0$.

The numerical analysis of the stability condition, $V_{eff,rr} > 0$, is depicted in Fig.6.3. The green region contains only stable orbits whereas the yellow region corresponds to unstable orbits. For comparison, we include the limiting values of the Schwarzschild spacetime. We see that the quadrupole parameter q changes the value of the minimum allowed radius ($3m$) and of the inner most stable circular orbit radius ($6m$) of the Schwarzschild metric. In fact, the quadrupole leads to the appearance of a second stable region below and over the radius $3m$, which is not present in the Schwarzschild limiting case. This region can reach the value of $r/m \approx 1$, approaching the singularity which is located at $r = m$. Moreover, within the spacetime determined by the interval

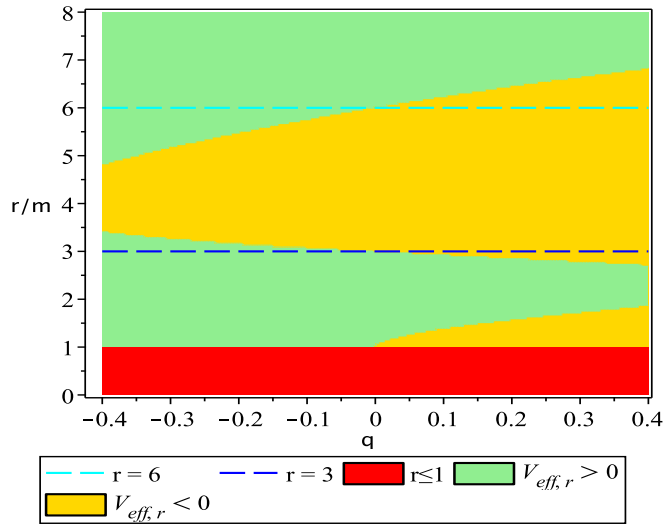

Figure 6.3: Stability analysis of circular orbits with radius r/m for different values of the quadrupole parameter q. Green (yellow) points represent stable (unstable) orbits. The red region lies inside the singularity.

$r \in (m, 2m]$, we notice that most of this region allows the existence of stable circular orbits with a disjoint region of instability for positive values of q.

Furthermore, the energy of test particles on circular orbits can be expressed as

$$E^2 = \frac{\epsilon\,(r-2m)^2}{r\,(r-3m)}\left[1 - \frac{mq\,(r-6m)}{2\,(r-m)\,(r-3m)}\right]. \tag{6.4.17}$$

In Fig. 6.4, we plot the regions in which the energy E^2 and angular momentum l^2 are both positive or negative simultaneously. The red region denotes all the radii that are not allowed for circular orbits because either the squared of the energy or of the angular momentum are negative. A comparison with Fig. 6.3 shows that the region contained between the singularity $r/m = 1$ and around $r/m = 3$ is allowed for circular orbits by the stability condition but is excluded by the energy and angular momentum conditions.

We conclude that the effect of the quadrupole on the properties of circular orbits is as follows. A positive quadrupole leads to an increase of the minimum allowed radius whereas a negative quadrupole generates the opposite effect. This means that only in the case of an oblate object, test particles are allowed to exist on orbits closer

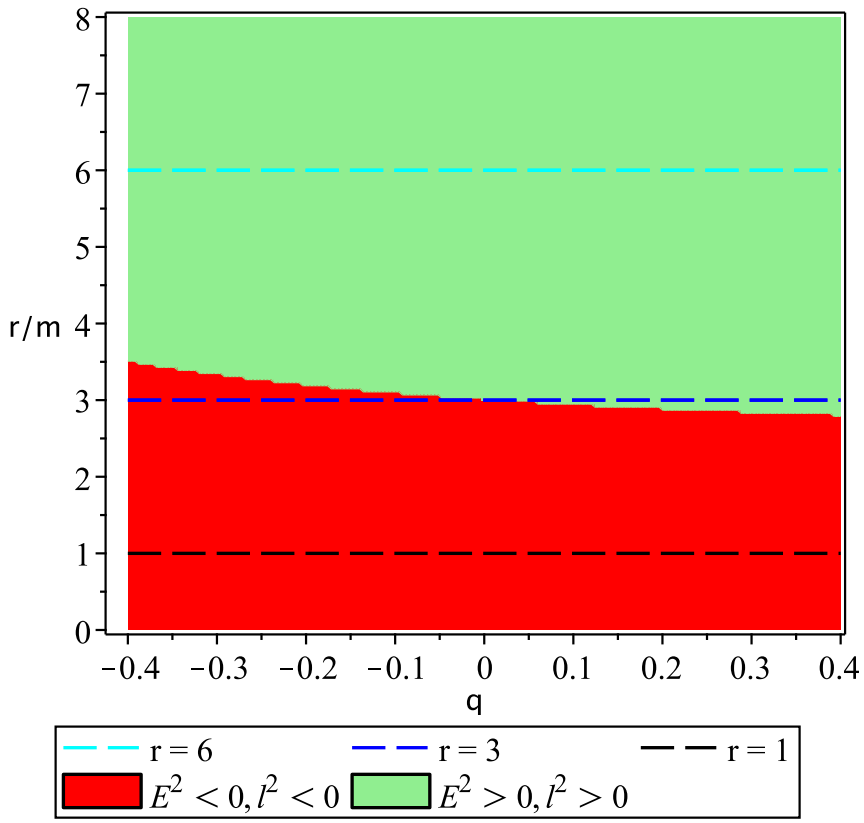

Figure 6.4: Energy E^2 and angular momentum l^2 of test particles on circular orbits in terms of the radius r/m and the quadrupole parameter q.

to the singularity, which is situated at $r = m$.

Finally, we consider the angular velocity

$$\begin{aligned} \Omega(r) = & \frac{d\varphi}{dt} = \frac{\dot{\varphi}}{\dot{t}} \\ = & \sqrt{\frac{m}{r^3}}\left[1 + \frac{q\,(r-4m)}{4\,(r-m)}\right], \end{aligned} \tag{6.4.18}$$

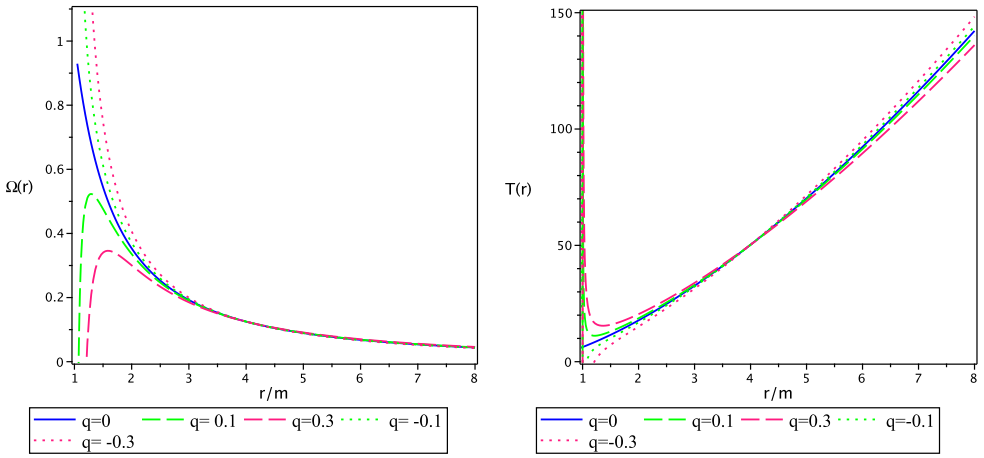

Figure 6.5: Angular velocity and period of circular orbits in terms of the radius r/m and the quadrupole parameter q.

and the period

$$\begin{aligned} T(r) &= \int \frac{\dot{t}}{\dot{\varphi}} d\varphi = 2\pi \frac{dt}{d\varphi} \\ &= 2\pi \sqrt{\frac{r^3}{m}} \left[1 - \frac{q\,(r-4m)}{4\,(r-m)} \right], \end{aligned} \tag{6.4.19}$$

of circular orbits. The behavior of the angular velocity and period are depicted in Fig. (6.5). We can see that the influence of the quadrupole on the value of the angular velocity increases as the radius of the orbit approaches the value of $r \approx 3m$. This agrees with the behavior of the stability condition and the energy and angular momentum shown in Figs. 6.3 and 6.4, respectively. For a given orbit radius, the angular velocity increases (decreases) for positive (negative) values of the quadrupole. Notice that close to the singularity located at $r = m$, there is a region in which the angular velocity is a well behaved function of q and r. This region corresponds to the stability region that was also found in Fig. 6.3.

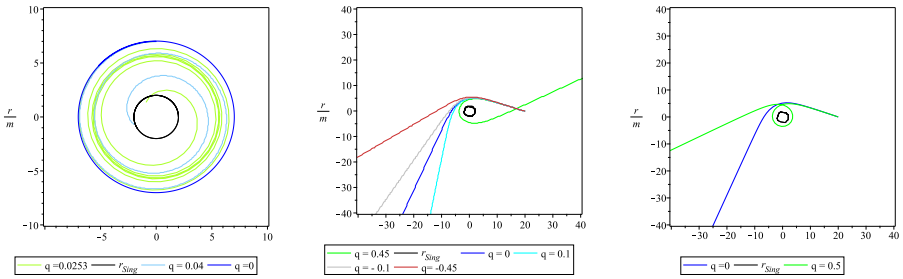

Figure 6.6: Influence of the quadrupole on unbounded orbits. Initial conditions: $\varphi(0) = \pi/2$, $r(0) = 7$, $\dot{\varphi}(0) = 0.07145$, $\dot{r}(0) = 0$ (top, left); $\varphi(0) = 0$, $r(0) = 20$, $\dot{\varphi}(0) = 0.04305$, $\dot{r}(0) = -2.5$ (top, right); $\varphi(0) = 0$, $r(0) = 20$, $\dot{\varphi}(0) = 0.04305$, $\dot{r}(0) = -2.489$ (bottom) ;

6.4.2 Bounded and unbounded orbits

We now study the influence of the quadrupole on the trajectories of massive test particles, moving along unbounded paths on the equatorial plane. The geodesics for different values of the quadrupole parameter are given in Figs. 6.6-6.7, where the radial coordinate is dimensionless (r/m).

We consider first unbounded Schwarzschild trajectories with non-zero initial radial velocities under the influence of the quadrupole. In this case, we see that for the chosen initial angular and radial velocities all the particles escape from the gravitational field of central slightly deformed body. This is illustrated Fig.6.6. The direction along which the particle escapes to infinity depends on the value of the quadrupole. It is worth noticing that, in principle, this effect could be used to measure the quadrupole of the central mass distribution.

In Fig. 6.7, we consider a Schwarzschild bounded orbit with zero initial radial velocity and the same non-zero value for the initial angular velocity. The left panel shows the Schwarzschild geodesic. The central and right panels illustrate the influence of a negative and positive small quadrupole, respectively. We conclude that that the small quadrupole does not affect the bounded character of the geodesic, but it does drastically modify the morphology of the trajectories.

We conclude that the quadrupole always affects the Schwarzschild trajectories. The explicit modifications depend on the properties of the original Schwarzschild trajectory and the value of the quadrupole parameter.

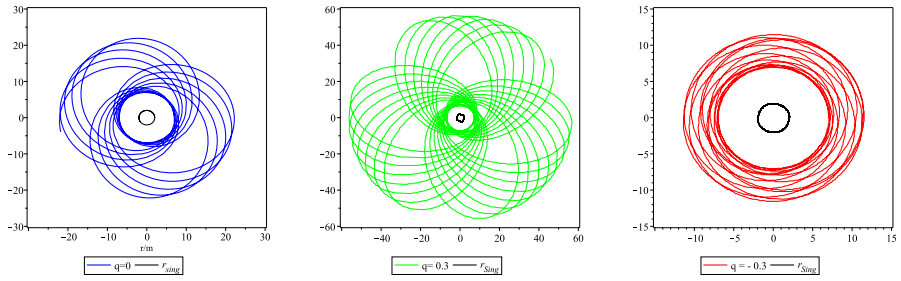

Figure 6.7: Influence of the quadrupole on Schwarzschild bounded orbits with vanishing initial radial velocity ($\dot{r}(0) = 0$). The initial conditions are $\varphi(0) = 0$, $r(0) = 7$, and $\dot{\varphi}(0) = 0.08$ for all the trajectories.

6.4.3 Radial geodesics and repulsive gravity

We now study the free fall of test particles. To this end, we consider the geodesics equations in their most general form as given in Eqs.(6.4.3)-(6.4.6). The important point is that in all the cases to be considered all the initial spatial velocities are assumed to vanish. The starting point can be chosen arbitrarily, but some special values of the angle θ are of interest, namely, the symmetry axis $\theta = 0$, the equatorial plane $\theta = \pi/2$, and some other different value that we can choose as $\theta = \pi/4$. In fact, in [**?**], it was shown that by analyzing the behavior of radial geodesics one can detect the presence of repulsive gravity [8, 28, 29]

A free falling particle will continue its motion along the radial direction, unless a force acts on it and changes the original radial direction. This phenomenon has been reported in the case of an exact solution with quadrupole moment in [**?**].

We will now consider the same situation in the case of the approximate solution we are analyzing in this work. The result of the integration of the geodesic equations (6.4.3)-(6.4.6) is illustrated in Fig. 6.8. We see that, in fact, free falling particles move along the original directions ($\theta = 0$, $\theta = \pi/4$, and $\theta = \pi/2$), independently of the value of quadrupole parameter q. This means that no repulsive gravity effects can be detected in the case of the approximate metric. Taking into account also the result of [**?**], we conclude that repulsive effects are non-linear, i.e., they appear only in the case of an exact quadrupolar metric.

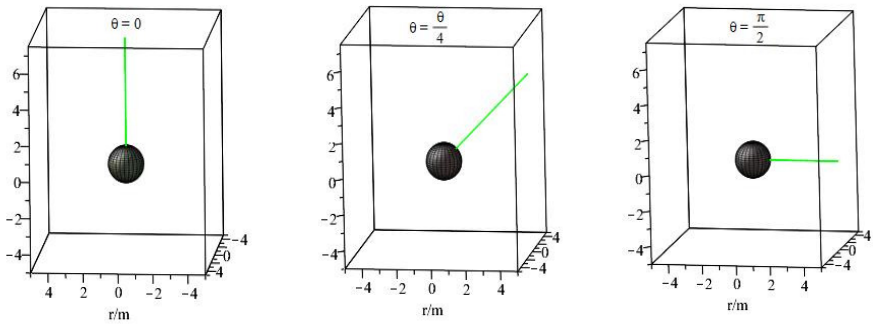

Figure 6.8: Free fall of test particles with vanishing initial velocities. On the axes $\theta = 0$ (top, left), $\theta = \pi/4$ (top, right), and $\theta = \pi/2$ (bottom). The sphere represents the singularity at the radius $r = m$ (top). The trajectories of the free falling test particles do not depend on the value of the parameter q. For concreteness, we set the energy of the test particle as $E = 1$.

6.5 Conclusions and remarks

In this work, we have derived a family of approximate vacuum solutions of Einstein equations with quadrupole. Among all the solutions contained in this family we choose a particular one, which presents a naked singularity at the hypersurface $r = m$, instead of $r = 2m$ as in other quadrupolar metrics. To our knowledge this is the only metric with such a singularity.

By applying an appropriate coordinate transformation, we found the Newtonian limit of the approximate solution and showed that it corresponds to the gravitational potential of a mass with quadrupole.

Then, we investigated the motion of test particles along circular orbits. We established that a positive quadrupole leads to an increase of the minimum allowed radius whereas a negative quadrupole generates the opposite effect. This means that only in the case of an oblate object, test particles are allowed to exist on orbits closer to the singularity, which is situated at $r = m$. In the case of bounded and unbounded trajectories, we found that the quadrupole always affects the Schwarzschild trajectories. The explicit modifications depend on the properties of the original Schwarzschild trajectory and the value of the quadrupole parameter.

Finally, we analyzed radial geodesics that have been used previously to detect effects of repulsive gravity in an exact quadrupolar metric. However, in the case of the approximate solution no repulsive effects were found. We conclude that repulsive gravity in the quadrupolar naked singularities is a non-linear phenomenon.

7 Darmois matching and C^3 matching

7.1 Introduction

The problem of matching two spacetimes across a surface Σ has been investigated for a long time [25]. In 1927, Darmois [7] proposed that a physically meaningful matching can be obtained by demanding that the first and second fundamental forms (induced metric and extrinsic curvature, respectively) be continuous across Σ. Later on, in 1955, Lichnerowicz [27] proposed an alternative approach that turned out to be equivalent to the Darmois approach by choosing the underlying coordinates appropriately. If the fundamental forms are not continuous across the matching surface, Israel proposed in [23] to "cover" Σ with a shell, whose energy-momentum tensor takes care of the discontinuities. More recently, in 2012, one of us proposed in [43] the C^3 approach, which is completely different because it is based not upon the use of fundamental forms (C^2 quantities), but upon the behavior of the curvature eigenvalues and their derivatives. This approach has been applied in cosmology, and relativistic astrophysics [28, 30, 31].

Whereas the Darmois approach demands the continuity of the first and second fundamental forms across the matching surface, which should be specified a priori, the C^3 approach contains a criterium that allows us to determine the location of the matching surface. Indeed, the point is that the C^3 approach can be used to propose an invariant definition of repulsive gravity [30]. In cosmology, this definition has been shown to be very useful because it allows us to construct models that describe inflation and the observed accelerated expansion of the Universe as repulsive gravity effects. In relativistic astrophysics, the situation is different; no repulsive gravity effects have been detected so far at the astrophysical level. In the description of the gravitational field of compact astrophysical objects, we use this fact in the C^3 approach to match vacuum and non-vacuum exact solutions in such a way that no repulsive gravity effects appear. Indeed, the behavior of the curvature eigenvalues can be used to detect regions of repulsive gravity within the gravitational field of a compact object. The spatial derivatives of the eigenvalues indicate the exact location where repulsion sets up. Thus, in the C^3 approach, we "cover" the repulsion region

with a different spacetime in such a way that no repulsive gravity effects can appear.

In a previous work [16], we formulated in detail the C^3 matching approach in asymptotically flat spacetimes. For an arbitrary metric that satisfies Einstein equations with cosmological constant and energy-momentum tensor, we computed the general form of a 6×6 matrix, from which the curvature eigenvalues can be derived. The approach was applied in the case of vacuum, conformally flat, and perfect-fluid spacetimes. In the present work, we continue the investigation of C^3 approach. The main goal is to compare the Darmois and the C^3 approaches in concrete examples. Indeed, we consider spherically symmetric spacetimes and find the conditions under which the vacuum Schwarzschild spacetime can be matched with exact perfect fluid solutions. We will see that the results depend on the matching approach. In fact, in the three specific cases we will consider, it turns out that according to the Darmois approach the matching is possible whereas the conditions for a C^3 matching are not satisfied. This result indicates that the two approaches are entirely different. We discuss this contradictory result and argue that the difference can be explained by considering the physical properties of the perfect fluid solutions near the matching surface. We use this result as a motivation to propose a generalization of the C^3 matching procedure that allows to treat the case of discontinuities across the matching hypersurface.

This paper is organized as follows. In Sections 7.2 and 7.3, we review in detail the main aspects of the Darmois and C^3 matching approaches, respectively. Sec. 7.4 is devoted to the matching of the exterior Schwarzschild metric with three different perfect fluid solutions, namely, the Tolman III, Heintzmann II, and Buchdahl I spacetimes. We compare the results of applying both the Darmois and the C^3 matching approaches and establish that they lead to different results due to the presence of discontinuities of the perfect fluid parameters on the matching surface. To be able to handle such cases, we propose in Sec. 7.5 a generalization of the C^3 matching procedure. Finally, in Sec. 7.6, we sum up our results.

7.2 Darmois matching approach

In this section, we present the fundamental concepts related to the notion of hypersurfaces, which are essential for the description of the Darmois matching approach [45, 3, 15]. Let $(\mathcal{M}, \mathbf{g})$ represent a spacetime, where $\mathcal{M}$ is a real smooth (i.e. C^∞) manifold of dimension 4 and $\mathbf{g}$ a Lorentzian metric on $\mathcal{M}$ with signature $(-,+,+,+)$. We assume that $(\mathcal{M}, \mathbf{g})$ is time orientable and $\mathcal{M}$ can be represented as a family of three-dimesional hypersurfaces. On each hypersurface Σ, a 3-metric $\mathbf{fl}$ is induced. The

hypersurface Σ is said to be spacelike, if **fl** is definite positive (signature: $+,+,+$); timelike, if γ is Lorentzian (signature: $-,+,+$); or null, if **fl** is degenerate (signature: $0,+,+$). Accordingly, each hypersurface Σ defines a normal vector field $\mathbf{n} \in \mathcal{M}$, whose norm is $\varepsilon = -1,+1,0$, corresponding to a spacelike, timelike, or null hypersurface, respectively.

A timelike hypersurface can be specified by means of a spatial coordinate $x^1 =$ constant. Hence, on Σ, we can introduce a vector basis $\mathbf{e}_i = \{\mathbf{e}_0, \mathbf{e}_2, \mathbf{e}_3\}$ and the extrinsic curvature tensor $\mathbf{K}$ by

$$\mathbf{K}_{ij} \equiv -\mathbf{e}_j \cdot \nabla_i \mathbf{n} = -\,\mathbf{e}_j^{\alpha}\, \mathbf{n}_{\alpha;i}\,, \tag{7.2.1}$$

where ";" denotes the usual covariant derivative, $\mathbf{K}_{ij}$ denotes the components of the extrinsic curvature tensor $\mathbf{K}$ and $\mathbf{e}_j^{\alpha}$, $\alpha = 0,1,2,3$, the αth component of the vector $\mathbf{e}_j$.

Now we assume that it is possible to foliate the spacetime $(\mathcal{M}, \mathbf{g})$ into a family of slices corresponding to timelike hypersurfaces $(\Sigma|_{x^1})_{x^1\in\Re}$. Therefore, there exists a smooth and regular scalar field X on $\mathcal{M}$ such that on each hypersurface there is a level surface of this scalar field, i.e.,

$$\forall x^1 \in \Re,\ \Sigma_{x^1} \equiv \{p \in \mathcal{M}, X(p) = x^1\}.$$

Thus, the regularity character of X guarantees that the hypersufaces satisfy the condition

$$\Sigma_{x^1} \cap \Sigma_{\tilde{x}^1} \neq \emptyset \ \text{ for } \ x^1 \neq \tilde{x}^1.$$

Consequently, the foliation of timelike hypersurfaces Σ_{x^1} covers $\mathcal{M}$ in such a way that

$$\mathcal{M} = \bigcup_{x^1\in\Re} \Sigma_{x^1}.$$

We now introduce coordinates adapted to the foliation $(\Sigma|_{x^1})_{x^1\in\Re}$. On each timelike hypersurfce $\Sigma|_{x^1}$ one can introduce coordinates $x^i = (x^0, x^2, x^3)$, being x^0 a temporal coordinate whereas x^2 and x^3 are spacial coordinates.

If these coordinates vary smoothly between any two infinitesimally near timelike hypersurfaces, $\Sigma|_{x^1}$ and $\Sigma|_{x^1+\delta x^1}$, it is always possible to construct a well-behaved chart of coordinates in $\mathcal{M}$. Consequently, a metric tensor on two neighboring hypersurfaces can be given in the form

$$\gamma(x^0, x^1, x^2, x^3) \text{ and } \gamma(x^0, x^1 + \delta x^1, x^2, x^3),$$

respectively. Accordingly, the metric tensor on $\mathcal{M}$ can be decomposed as

$$g = \gamma_{ij}(\mathrm{d}\,x^i + \beta^i\,\mathrm{d}\,x^1) \otimes (\mathrm{d}\,x^j + \beta^j\,\mathrm{d}\,x^1) + N^2\,\mathrm{d}\,x^1 \otimes \mathrm{d}\,x^1 \tag{7.2.2}$$

where $\beta^i(x^\alpha)$ is determined by the relation

$$x^i(\Sigma|_{x^1+\delta x^1}) = x^i(\Sigma|_{x^1}) - \beta^i(x^\alpha)\delta x^1. \tag{7.2.3}$$

Here, $x^i(\Sigma|_{x^1+\delta x^1})$ are the coordinates of a point in $\Sigma|_{x^1+\delta x^1}$ constructed by a perpendicular line from the point $x^i(\Sigma|_{x^1})$ on $\Sigma|_{x^1}$ to $\Sigma|_{x^1+\delta x^1}$. We get then the following expressions for the metric components

$$\begin{pmatrix} g_{11} & g_{1i} \\ g_{i1} & g_{ij} \end{pmatrix} = \begin{pmatrix} \beta_i\beta^i + N^2 & \beta_i \\ \beta_i & \gamma_{ij} \end{pmatrix}, \tag{7.2.4}$$

and the components of the inverse metric are given by

$$\begin{pmatrix} g^{11} & g^{1i} \\ g^{j1} & g^{ij} \end{pmatrix} = \begin{pmatrix} 1/N^2 & -\beta^i/N^2 \\ -\beta^i/N^2 & \gamma^{ij} + \beta^i\beta^j/N^2 \end{pmatrix}, \tag{7.2.5}$$

where $\beta_i = \gamma_{ij}\beta^j$. Naturally, for a timelike hypersurface its normal vector $\mathbf{n}$ satisfies the condition $n^\alpha n_\alpha = 1$; then,

$$n_\alpha = (0, N, 0, 0), \tag{7.2.6}$$

$$n^\alpha = -(\beta^0, -1, \beta^2, \beta^3)/N. \tag{7.2.7}$$

The Darmois matching approach can be described as follows. Let Σ be a three-dimensional timelike hypersurface spliting the spacetime $(\mathcal{M}, \mathbf{g})$ in two 4-dimensional manifolds $(\mathcal{M}^-, \mathbf{g}^-)$ and $(\mathcal{M}^+, \mathbf{g}^+)$. The metric tensor $\mathbf{g}$ is of class C^3 except on the hypersurface Σ and satisfies the Einstein equations in $\mathcal{M}^-$ and $\mathcal{M}^+$, respectively. Darmois matching can be considered as a C^2-matching that includes the following conditions:

Condition 1: $\mathbf{fl}^-|_\Sigma = \mathbf{fl}^+|_\Sigma$ (i. e., $\mathbf{fl}$ is continuos across Σ) ,

Condition 2: The surface stress-energy tensor on Σ (defined to be the integral of $\mathbf{T}$ with respect to the "distance" Z measured perpendicularly through Σ) satisfies the condition

$$\lim_{\epsilon\to 0}\int_{-\epsilon}^{\epsilon}(\mathbf{T})^i{}_j\,\mathrm{d}\,Z = 0,$$

which yields to $\mathbf{K}^-|_\Sigma = \mathbf{K}^+|_\Sigma$ (i. e., $\mathbf{K}$ is continuous across Σ).

Accordingly, in summa, Darmois matching formalism consists of choosing an appropriate coordinate chart on which the metric tensor and the extrinsic curvature of the surface are continuous and match the corresponding solutions.

7.3 C^3 matching approach

The C^3 matching approach uses as a starting point the curvature eigenvalues, whose behavior does not depend on the choice or coordinates. This method was first proposed in relativistic astrophysics in [43] and further applied to define repulsive gravity in [30], to investigate cosmological models in [31, 14], and to study asymptotically flat spacetimes in [16].

For a given metric, there are several equivalent methods to calculate its curvature eigenvalues [46]. Here, we use the Cartan formalism of differential forms to emphasize the independence from the coordinates. Thus, consider a set of differential forms ϑ^a, $a = 0, ..., 3$ such that

$$ds^2 = g_{\mu\nu} dx^\mu \otimes dx^\nu = \eta_{ab} \vartheta^a \otimes \vartheta^b \,, \tag{7.3.1}$$

with $\eta_{ab} = diag(-1, 1, 1, 1)$, and $\vartheta^a = e^a{}_\mu dx^\mu$. The first and second Cartan equations

$$d\vartheta^a = -\omega^a{}_b \wedge \vartheta^b \,, \tag{7.3.2}$$

$$\Omega^a{}_b = d\omega^a{}_b + \omega^a{}_c \wedge \omega^c{}_b = \frac{1}{2} R^a{}_{bcd} \vartheta^c \wedge \vartheta^d \tag{7.3.3}$$

allow us to compute the components of the Riemann curvature tensor R_{abcd} in the local orthonormal frame ϑ^a. Furthermore, we introduce the bivector representation that consists in defining the curvature components R_{abcd} as the components of a 6×6 matrix R_{AB} according to the convention proposed in [34], which establishes the following correspondence between tetrad ab and bivector indices A:

$$01 \to 1 \,, \quad 02 \to 2 \,, \quad 03 \to 3 \,, \quad 23 \to 4 \,, \quad 31 \to 5 \,, \quad 12 \to 6 \,. \tag{7.3.4}$$

Due to the symmetry $R_{abcd} = R_{cdab}$, the matrix R_{AB} is symmetric with 21 independent components. The algebraic Bianchi identity $R_{a[bcd]} = 0$, which in bivector representation reads

$$R_{14} + R_{25} + R_{36} = 0 \tag{7.3.5}$$

reduces the number of independent components to 20. Furthermore, Einstein's equations

$$R_{ab} - \frac{1}{2} R \eta_{ab} = k\, T_{ab}\,, \quad R_{ab} = R^{c}{}_{acb}\,, \tag{7.3.6}$$

can be written explicitly in terms of the curvature components R_{AB}, resulting in a set of ten algebraic equations that relate the components of R_{AB} and T_{ab}. Consequently, only ten components R_{AB} are algebraic independent and can be arranged in the 6×6 curvature matrix in the following way

$$R_{AB} = \begin{pmatrix} M_1 & L \\ L & M_2 \end{pmatrix}, \tag{7.3.7}$$

where

$$L = \begin{pmatrix} R_{14} & R_{15} & R_{16} \\ R_{15} - \kappa T_{03} & R_{25} & R_{26} \\ R_{16} + \kappa T_{02} & R_{26} - \kappa T_{01} & -R_{14} - R_{25} \end{pmatrix},$$

and M_1 and M_2 are 3×3 symmetric matrices

$$M_1 = \begin{pmatrix} R_{11} & R_{12} & R_{13} \\ R_{12} & R_{22} & R_{23} \\ R_{13} & R_{23} & -R_{11} - R_{22} + \kappa \left(\frac{T}{2} + T_{00}\right) \end{pmatrix},$$

$$M_2 = \begin{pmatrix} -R_{11} + \kappa \left(\frac{T}{2} + T_{00} - T_{11}\right) & -R_{12} - \kappa T_{12} & -R_{13} - \kappa T_{13} \\ -R_{12} - \kappa T_{12} & -R_{22} + \kappa \left(\frac{T}{2} + T_{00} - T_{22}\right) & -R_{23} - \kappa T_{23} \\ -R_{13} - \kappa T_{13} & -R_{23} - \kappa T_{23} & R_{11} + R_{22} - \kappa T_{33} \end{pmatrix},$$

with $T = \eta^{ab} T_{ab}$. This is the most general form of a curvature tensor that satisfies Einstein's equations with an arbitrary energy-momentum tensor. The eigenvalues λ_n, $n = 1, ..., 6$ of the matrix R_{AB} are known as the curvature eigenvalues.

The C^3 matching approach can be formulated as follows. Let $(\mathcal{M}^-, g^-)$ and $(\mathcal{M}^+, g^+)$ be an arbitrary and an asymptotically flat spacetime, respectively, which satisfy Einstein equations. Let λ_n^- and λ_n^+ be the corresponding curvature eigenvalues. Let r be a spatial coordinate associated with the asymptotic flatness property of $(\mathcal{M}^+, g^+)$. Then, the C^3 matching approach can be split into two steps:

Step 1: Define the matching surface Σ as determined by the matching radius

$$r_{match} \in [r_{rep}, \infty) \,, \quad with \quad r_{rep} = max\{r_l\} \,, \quad \left.\frac{\partial \lambda_i^+}{\partial r}\right|_{r=r_l} = 0 \,. \tag{7.3.8}$$

Step 2: Match the spacetimes $(\mathcal{M}^-, \mathbf{g}^-)$ and $(\mathcal{M}^+, \mathbf{g}^+)$ at Σ by imposing the conditions

$$[\lambda_n] = \lambda_n^- - \lambda_n^+ \quad \forall\, n \,, \tag{7.3.9}$$

where $[\lambda_n]$ denotes the jump of the corresponding eigenvalue across the matching surface Σ.

From a pragmatical point of view, the interior region of compact objects corresponds to the spacetime $(\mathcal{M}^-, \mathbf{g}^-)$ whereas the exterior region is described by $(\mathcal{M}^+, \mathbf{g}^+)$.

7.4 Matching spherically symmetric spacetimes

In this section, we will apply the Darmois and C^3 matching approaches to three different perfect fluid spherically symmetric spacetimes.

Regarding the Darmois approach, we will consider the case of a normal vector $\mathbf{n}$ as given in Eq.(7.2.6). Then, the extrinsic curvature $\mathbf{K}$ can be expressed as

$$\mathbf{K}_{ij} = -\mathbf{n}_{j;i} = \frac{1}{2N}\left(N_{i,j} + N_{j,i} - h_{ij,1} - 2N_k\Gamma^k_{ij}\right) \,. \tag{7.4.1}$$

Additionally, we restrict ourselves to spacetiems with metric

$$g = \mathbf{fl}_{ii}\, \mathrm{d}\, x^i \otimes \mathrm{d}\, x^i + N^2\, \mathrm{d}\, x^1 \otimes \mathrm{d}\, x^1, \tag{7.4.2}$$

so that the components of K reduce to

$$\mathbf{K}_{ij} = -\frac{1}{2N}\mathbf{fl}_{ij,1} \,, \quad i,j = 0,2,3 \,. \tag{7.4.3}$$

Moreover, in the interior and exterior regions, we choose spherical coordinates and metrics of the form

$$g = -G\, \mathrm{d}\, t \otimes \mathrm{d}\, t + \frac{1}{F}\, \mathrm{d}\, r \otimes \mathrm{d}\, r + H\, \mathrm{d}\, \Omega \otimes \mathrm{d}\, \Omega \tag{7.4.4}$$

where $\mathrm{d}\,\Omega \otimes \mathrm{d}\,\Omega \equiv \mathrm{d}\,\theta \otimes \mathrm{d}\,\theta + \sin^2\theta\,\mathrm{d}\,\phi \otimes \mathrm{d}\,\phi$ and the functions G, F, and H depend on r only. Similarly, we suppose that the conventional matter governing the internal spacetime dynamics is a perfect fluid determined by the energy-momentum tensor

$$\mathbf{T}^{\alpha\beta} = (\rho + p)\mathbf{V}^{\alpha}\mathbf{V}^{\beta} + p\mathbf{g}^{\alpha\beta} \tag{7.4.5}$$

where ρ and p are the energy density and the pressure of the fluid, respectively, and $\mathbf{V}$ is the velocity of the fluid, which we choose as the comoving velocity $\mathbf{V}\alpha = (-1, 0, 0, 0)$.

According to Birkhoff's theorem, the exterior spacetime must be described by the Schwarzschild metric

$$g^{+} = -\left(1 - \frac{2m}{r}\right)\mathrm{d}\,t \otimes \mathrm{d}\,t + \left(1 - \frac{2m}{r}\right)^{-1}\mathrm{d}\,r \otimes \mathrm{d}\,r + r^2\,\mathrm{d}\,\Omega \otimes \mathrm{d}\,\Omega. \tag{7.4.6}$$

Furthermore, we choose the matching hypersurface as a sphere of constant radius. Hence, according to equations (7.4.2) and (7.4.3), the metric tensor induced on Σ and its extrinsic curvature are given by

$$\mathbf{fl}^{+}_{tt} = -1 + \frac{2m}{r}\,, \quad \mathbf{fl}^{+}_{\theta\theta} = r^2\,, \quad \mathbf{fl}^{+}_{\phi\phi} = r^2\sin^2\theta\,, \tag{7.4.7}$$

and

$$\mathbf{K}^{+}_{tt} = \frac{m}{r^2}\left(1 - \frac{2m}{r}\right)^{1/2}\,, \quad \mathbf{K}^{+}_{\theta\theta} = -r\left(1 - \frac{2m}{r}\right)^{1/2}\,, \quad \mathbf{K}^{+}_{\phi\phi} = \sin^2\theta\,\mathbf{K}^{+}_{\theta\theta}, \tag{7.4.8}$$

respectively.

For the C^3 approach we only need to calculate the curvature eigenvalues. We choose the orthonormal tetrad ϑ^a as

$$\vartheta^0 = \left(1 - \frac{2m}{r}\right)^{1/2}\mathrm{d}\,t\,,\ \vartheta^1 = \left(1 - \frac{2m}{r}\right)^{-1/2}\mathrm{d}\,r\,,\ \vartheta^2 = r\,\mathrm{d}\,\theta\,,\ \vartheta^3 = r\sin\theta\ \mathrm{d}\,\phi\,. \tag{7.4.9}$$

A straightforward computation shows that the curvature matrix R_{AB} is diagonal and the eigeinvalues are

$$\lambda^{+}_2 = \lambda^{+}_3 = -\lambda^{+}_5 = -\lambda^{+}_6 = m/r^3, \tag{7.4.10}$$

$$\lambda^{+}_1 = -\lambda^{+}_4 = -2m/r^3. \tag{7.4.11}$$

We can now perform the first step of the C^3 approach, which consists in finding the extrema of the exterior eigenvalues. Obviously, none of the Schwarzchild eigenvalues has an extremum. This means that there is no repulsion radius r_{rep}, which indicates in the approach the smallest sphere at which the matching can be carried out. Consequently, there is no repulsion region in the Schwarzschild spacetime that should be covered by an interior solution, which is the conceptual background of the C^3 approach. Then, the matching radius can be located anywhere outside the central singularity, i.e., $r_{match} \in (0, \infty)$.

7.4.1 The Tolman III spacetime

The Tolman III spacetime is an exact solution of Einstein equations that describes a perfect fluid with constant energy density. It can be written out as

$$g^- = -\left[\frac{3}{2}f(K) - \frac{1}{2}f(r)\right]^2 \mathrm{d}\,t \otimes \mathrm{d}\,t + \frac{1}{f^2(r)}\,\mathrm{d}\,r \otimes \mathrm{d}\,r + r^2\,\mathrm{d}\,\Omega \otimes \mathrm{d}\,\Omega\,, \tag{7.4.12}$$

$$\rho = \frac{3m}{4\pi K^3}\,, \quad p = \frac{3m}{4\pi K^3}\frac{[f(r) - f(K)]}{[3f(K) - f(r)]}\,, \quad f(r) = \left(1 - \frac{2mr^2}{K^3}\right)^{1/2}\,, \tag{7.4.13}$$

where m and K are constants. Furthermore, the components of the metric on Σ are given by

$$\gamma^-_{tt} = -\left[\frac{3}{2}f(K) - \frac{1}{2}f(r)\right]^2\,,\ \gamma^-_{\theta\theta} = r^2\,,\ \gamma^-_{\phi\phi} = r^2\sin^2\theta\,, \tag{7.4.14}$$

and the components of the corresponding extrinsic curvature become

$$\mathbf{K}^-_{tt} = \frac{rm}{2K^{9/2}}[3K(K-2m)^{1/2} - (K^3 - 2mr^2)^{1/2}]\,,$$
$$\mathbf{K}^-_{\theta\theta} = -\frac{r}{K^{3/2}}(K^3 - 2mr^2)^{1/2}\,, \mathbf{K}^-_{\phi\phi} = \sin^2\theta\mathbf{K}^-_{\theta\theta}\,. \tag{7.4.15}$$

Consider now the matching hypersurface Σ as a sphere of radius $r = r_0 = \text{const}$. Then, by imposing the first Darmois condition on the exterior (7.4.14) and interior (7.4.7) metrics, it follows that

$$\mathbf{fl}^+|_{r=r_0} = \mathbf{fl}^-|_{r=r_0}\,, \tag{7.4.16}$$

only if $K = r_0$. Furthermore, a comparison of the components of the extrinsic curvature (7.4.15) and (7.4.8) leads to

$$\mathbf{K}^+|_{r=r_0} = \mathbf{K}^-|_{r=r_0} \,, \tag{7.4.17}$$

implying that the second Darmois condition is satisfied identically. We conclude that according to Darmois approach, the exterior Schwarzschild metric and the interior Tolman III solution can be matched on the hypersurface $r = r_0 = \text{const.}$ and, consequently, determine a physically meaningful spacetime. Notice that on the matching hypersurface $r = r_0$, the pressure vanishes, but the density remains constant, $\rho(r_0) = 3m/4\pi r_0^3$.

Consider now the C^3 matching approach. The choice of the differential forms ϑ^a is suggested by the diagomal form of the metric (7.4.12). Then,

$$\vartheta^0 = \left[\frac{3}{2}f(K) - \frac{1}{2}f(r)\right] \mathrm{d}\, t \,, \tag{7.4.18}$$

$$\vartheta^1 = \frac{1}{f(r)}\, \mathrm{d}\, r \,,\ \vartheta^2 = r\, \mathrm{d}\, \theta \,,\ \vartheta^3 = r\, \mathrm{d}\, \phi \,. \tag{7.4.19}$$

The computation of the corresponding matrix R_{AB} yields the following curvature eigenvalues

$$\lambda_1^- = \lambda_2^- = \lambda_3^- = \frac{2m(K^3 - 2mr^2)^{1/2}}{K^3[3K(K-2m)^{1/2} - (K^3 - 2mr^2)^{1/2}]} \,, \tag{7.4.20}$$

$$\lambda_4^- = -\lambda_1^- + 4\pi(\rho + p) = \frac{2m}{K^3} \,, \tag{7.4.21}$$

$$\lambda_5^- = -\lambda_2^- + 4\pi(\rho + p) = \frac{2m}{K^3} \,, \tag{7.4.22}$$

$$\lambda_6^- = -\lambda_3^- + 4\pi(\rho + p) = \frac{2m}{K^3} \,. \tag{7.4.23}$$

The second step of the C^3 matching approach implies that on the matching hypersurface, $r = r_{match}$, all the eigenvalues should coincide, $\lambda_n^+ = \lambda_n^-$, $\forall\, n$. A comparison of the above expressions with the Schwarzschild eigenvalues (7.4.10) shows that there is no r_{match} for which all the conditions are satisfied. We conclude that according to the C^3 matching approach, the interior Tolman III solution cannot be matched with

the exterior Schwarzschild metric.

7.4.2 The Heintzmann II spacetime

The Heintzmann II spacetime is a perfect fluid solution of Einstein equations described by the metric [9]

$$g^- = -A^2(1+ar^2)^3\,\mathrm{d}\,t\otimes\mathrm{d}\,t + \left\{1-\frac{3ar^2}{2(1+ar^2)}\left[1+K(1+4ar^2)^{-1/2}\right]\right\}^{-1}\mathrm{d}\,r\otimes\mathrm{d}\,r + r^2\,\mathrm{d}\,\Omega\otimes\mathrm{d}\,\Omega\,, \tag{7.4.24}$$

$$p = -\frac{3a\left[(7ar^2+1)K+3(ar^2-1)(4ar^2+1)^{1/2}\right]}{16\pi(4ar^2+1)^{1/2}(ar^2+1)^2}, \tag{7.4.25}$$

$$\rho = \frac{3a\left[3(3ar^2+1)K+(4a^2r^4+13ar^2+3)(4ar^2+1)^{1/2}\right]}{16\pi(4ar^2+1)^{3/2}(ar^2+1)^2}\,, \tag{7.4.26}$$

where a, A and K are constants.

This metric tensor induces on a hypersurface Σ with r =const. a 3-metric with extrinsic curvature given by

$$\mathbf{fl}^-_{tt} = -A^2(ar^2+1)^3, \quad \mathbf{fl}^-_{\theta\theta} = r^2\,, \quad \mathbf{fl}^-_{\phi\phi} = r^2\sin^2\theta\,, \tag{7.4.27}$$

and

$$\begin{aligned}
\mathbf{K}^-_{tt} &= -\frac{3\sqrt{2}A^2ar(ar^2+1)^{3/2}}{2(4ar^2+1)^{1/4}}\left[(2-ar^2)(4ar^2+1)^{1/2}-3ar^2K\right]^{1/2}\,,\\
\mathbf{K}^-_{\theta\theta} &= \frac{\sqrt{2}r}{2(ar^2+1)^{1/2}(4ar^2+1)^{1/4}}\left[(2-ar^2)(4ar^2+1)^{1/2}-3ar^2K\right]^{1/2}\,,\\
\mathbf{K}^-_{\phi\phi} &= \sin^2\theta\mathbf{K}^-_{\theta\theta}\,.
\end{aligned} \tag{7.4.28}$$

We now consider as matching hypersurface a sphere of radius $r = r_0$, where we impose the Darmois conditions $\mathbf{fl}^-|_{r=r_0} = \mathbf{fl}^+|_{r=r_0}$ and $\mathbf{K}^-|_{r=r_0} = \mathbf{K}^+|_{r=r_0}$. Lengthy calculations show that in this case Darmois conditions are equivalent to fixing the

arbitrary constants that enter the spacetime metric as

$$a = -\frac{m}{(7m-3r_0)r_0^2}\,, A = -\frac{3^{1/2}(3r_0-7m)^{3/2}}{r_0^{1/2}(18m-9r_0)}\,, K = -\frac{3^{1/2}(8m-3r_0)(m-r_0)^{1/2}}{r_0(7m-3r_0)}, \tag{7.4.29}$$

in terms of the Schwarzschild mass m and the radius of the matching sphere r_0. We conclude that according to Darmois approach the Heintzmann II spacetime can be matched with the exterior Schwarzschild metric.

We notice that if we introduce the above values for the constants a, A, and K into the expressions for the pressure and density of the Heintzmann solution, we obtain that on the matching hypersurface, the pressure vanishes, but the density is different from zero. In fact, the density tends to zero only asymptotically. We illustrate this behavior in Fig. 7.1, where for concreteness we set $r_0 = 3$. We see that the pressure is positive inside the source, $0 < r_0 < 3$, vanishes on the matching hypersurface, $r_0 = 3$, and becomes negative outside the body. On the other hand, the density is always positive and vanishes only asymptotically.

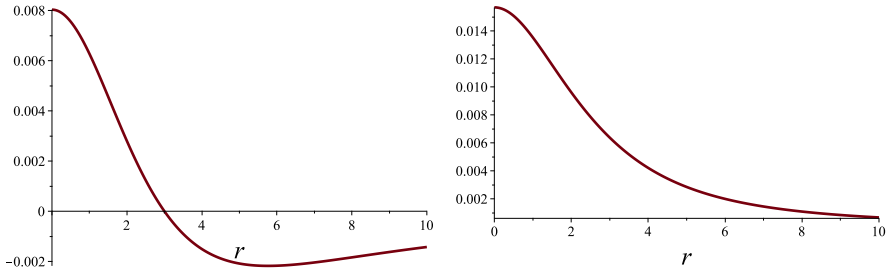

Figure 7.1: Pressure and the energy density of the Heintzmann II solution for $r_0 = 3$ and $m = 1$.

To apply the C^3 approach, we choose the orthonormal tetrad as

$$\vartheta^0 = A(1+ar^2)^{3/2}\,\mathrm{d}\,t\,,\ \vartheta^2 = r\,\mathrm{d}\,\theta\,,\ \vartheta^3 = r\,\mathrm{d}\,\phi\,, \tag{7.4.30}$$

$$\vartheta^1 = \left\{1 - \frac{3ar^2}{2(1+ar^2)}\left[1+K(1+4ar^2)^{-1/2}\right]\right\}^{-1/2}\mathrm{d}\,r\,, \tag{7.4.31}$$

which leads to the curvature eigenvalues

$$\lambda_1^- = -\frac{3a[3aKr^2(3ar^2+1)+(4ar^2+1)^{1/2}(4a^2r^4-3ar^2-1)]}{(4ar^2+1)^{3/2}(ar^2+1)^2}\,, \tag{7.4.32}$$

$$\lambda_2^- = \lambda_3^- = -\frac{3a[(ar^2-2)(4ar^2+1)^{1/2}+3aKr^2]}{2(4ar^2+1)^{1/2}(ar^2+1)^2}\,, \tag{7.4.33}$$

$$\lambda_4^- = -\lambda_1^- + 4\pi(\rho+p) = \frac{3a[(4ar^2+1)^{1/2}+K]}{2(4ar^2+1)^{1/2}(ar^2+1)}\,, \tag{7.4.34}$$

$$\begin{aligned}\lambda_5^- &= -\lambda_2^- + 4\pi(\rho+p)\\ &= -\frac{3a[2Kar^2(ar^2-1)-(4ar^2+1)(4ar^2+1)^{1/2}-K]}{2(4ar^2+1)^{3/2}(ar^2+1)^2}\,,\end{aligned} \tag{7.4.35}$$

$$\begin{aligned}\lambda_6^- &= -\lambda_3^- + 4\pi(\rho+p) =\\ &= -\frac{3a[2Kar^2(ar^2-1)-(4ar^2+1)(4ar^2+1)^{1/2}-K]}{2(4ar^2+1)^{3/2}(ar^2+1)^2}\,.\end{aligned} \tag{7.4.36}$$

It is then possible to prove that there is no solution to the C^3 matching condition, which implies the equality between the interior and exterior eigenvalues. This incompatibility is illustrated in Fig. 7.2, where we plot the eigenvalues of the Heintzmann II metric for a, A, and K given by (7.4.29) and the eigenvalues of the Schwarzschild metric with $m = 1$ and $r_0 = 3$.

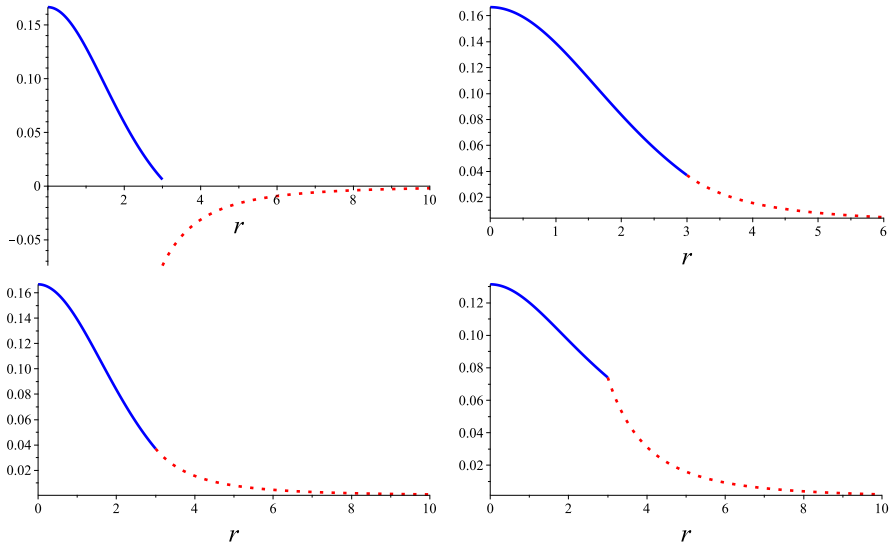

Figure 7.2: The Eigenvalues of the Heintzmann II metric ($r \leq 3$) and of the Schwarzschild metric ($r \geq 3$) for $r_0 = 3$ and $m = 1$.

7.4.3 The Buchdahl I spacetime

The Buchdahl spacetime describres a spherically symmetric perfect fluid solution of Einstein equations. The corresponding metric, density, and pressure read [9]

$$g^- = -A[(1+Kr^2)^{3/2} + B(2-Kr^2)^{1/2}(5+2Kr^2)]^3\,\mathrm{d}t\otimes\mathrm{d}t + \frac{2(1+Kr^2)}{2-Kr^2}\,\mathrm{d}r\otimes\mathrm{d}r + r^2\,\mathrm{d}\Omega\otimes\mathrm{d}\Omega\,, \tag{7.4.37}$$

$$\rho = \frac{3K(Kr^2+3)}{16\pi(Kr^2+1)^2}\,, \tag{7.4.38}$$

$$p = -\frac{9K}{16\pi}\frac{B(Kr^2+1)^{1/2}(2-Kr^2)^{1/2}(2Kr^2+1)+K^2r^4-1}{(Kr^2+1)^{3/2}[B(2Kr^2+5)(2-Kr^2)^{1/2}+(Kr^2+1)^{3/2}]}\,, \tag{7.4.39}$$

where A, B, and K are arbitrary constants. On a hypersurface r =const., this metric induces the 3-metric

$$\mathbf{fl}^-_{tt} = -A[(Kr^2+1)^{3/2} + B(2Kr^2+5)(2-Kr^2)^{1/2}]^2, \tag{7.4.40}$$
$$\mathbf{fl}^-_{\theta\theta} = r^2\,, \quad \mathbf{fl}^-_{\phi\phi} = r^2\sin^2\theta\,,$$

whose extrinsic curvature is given by

$$\mathbf{K}^{-}_{tt} = \frac{3\sqrt{2}KAr(2-Kr^2)^{1/2}[(Kr^2+1)^{3/2}+B(2-Kr^2)^{1/2}(2Kr^2+5)]}{2(1+Kr^2)^{1/2}(2-Kr^2)^{1/2}} \times [B(1-2Kr^2)+(1+Kr^2)^{1/2}(2-Kr^2)^{1/2}], \tag{7.4.41}$$

$$\mathbf{K}^{-}_{\theta\theta} = \frac{\sqrt{2}(2-Kr^2)^{1/2}}{2(Kr^2+1)^{1/2}}, \qquad \mathbf{K}^{-}_{\phi\phi} = \sin^2\theta\,\mathbf{K}^{-}_{\theta\theta}.$$

Then, imposing the first and second Darmois conditions on a matching hypersurface determined by a sphere of radius $r = 2\kappa m$, we obtain that if we choose the arbitrary constants entering the metric as

$$A = \frac{(9\kappa^2+12\kappa+4)(\kappa-1)}{108\kappa^2(3\kappa-2)}, \tag{7.4.42}$$

$$B = \frac{\kappa^{1/2}(3\kappa-4)}{(2+3\kappa)(2\kappa-2)^{1/2}}, \tag{7.4.43}$$

$$K = \frac{1}{2\kappa^2 m^2(3\kappa-2)}, \tag{7.4.44}$$

then the Darmois matching approach guarantees that the interior Buchdahl I spacetime can be matched with the exterior Schwarzschild spacetime.

It can also be shown that at the matching radius $r = 2\kappa m$, the pressure vanishes identically and the density is nonzero and positive. This behavior is illustrated in Fig. 7.3.

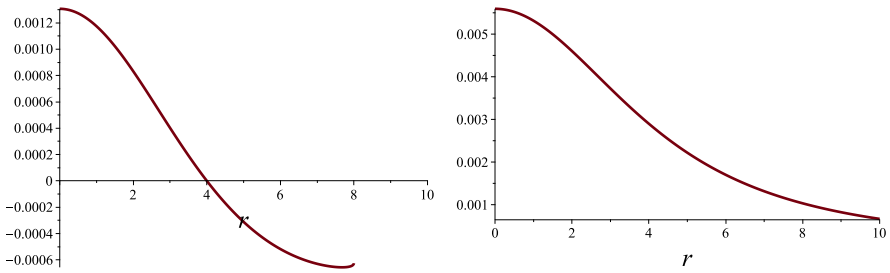

Figure 7.3: The pressure and the energy density of the Buchdahl I spacetime for $\kappa = 2$, $m = 1$, and matching radius located at $r = 4$.

To carry out the C^3 approach, we choose the orthonormal tetrad as

$$\vartheta^0 = A^{1/2}[(1+Kr^2)^{3/2} + B(2-Kr^2)^{1/2}(5+2Kr^2)]^{3/2}\,\mathrm{d}\,t\,, \tag{7.4.45}$$

$$\vartheta^1 = \left[\frac{2(1+Kr^2)}{2-Kr^2}\right]^{1/2} r\,\mathrm{d}\,r\,,\ \vartheta^2 = r\,\mathrm{d}\,\theta\,,\ \vartheta^3 = r\,\mathrm{d}\,\phi\,. \tag{7.4.46}$$

Then, following the method for calculating the curvature matrix R_{AB}, we find the following curvature eigenvalues

$$\lambda_1^- = \frac{3K[2(1-Kr^2)(1+Kr^2)^{3/2} + B(2-Kr^2)^{1/2}(1-4K^2r^4-6Kr^2)]}{2(1+Kr^2)^2[(1+Kr^2)^{3/2} + B(2-Kr^2)^{1/2}(5+2Kr^2)]}\,, \tag{7.4.47}$$

$$\lambda_2^- = \lambda_3^- = \frac{3K(2-Kr^2)^{1/2}[B(1-2Kr^2) + (1+Kr^2)^{1/2}(2-Kr^2)^{1/2}]}{2(1+Kr^2)[(1+Kr^2)^{3/2} + B(2-Kr^2)^{1/2}(5+2Kr^2)]} \tag{7.4.48}$$

$$\lambda_4^- = -\lambda_1^- + 4\pi(\rho+p) = \frac{3K}{2(Kr^2+1)}\,, \tag{7.4.49}$$

$$\lambda_5^- = -\lambda_2^- + 4\pi(\rho+p) = \frac{3K}{2(Kr^2+1)^2}\,, \tag{7.4.50}$$

$$\lambda_6^- = -\lambda_3^- + 4\pi(\rho+p) = \frac{3K}{2(Kr^2+1)^2}\,. \tag{7.4.51}$$

Then, it can be shown that no solution exists for the C^3 matching condition. In fact, the equivalence between the interior and exterior curvature eigenvalues on the matching surface can be reached only for some of the eigenvalues. To illustrate the lack of coincidence, we plot in Fig. 7.4, the behavior of the eigenvalues as functions of the radial coordinate r. For concreteness, the free parameters A, B and K are chosen as given in Eq.(7.4.42) with $\kappa = 2$ and $m = 1$.

7.4.4 Analysis of the results

The results of the previous subsections show that different matching approaches can lead to different results. Whereas according to the Darmois approach, it is possible to match the exterior Schwazschild solution with the Tolman III, Heintzmann II, and Buchdahl I perfect fluid solutions, the C^3 matching approach shows that it is not

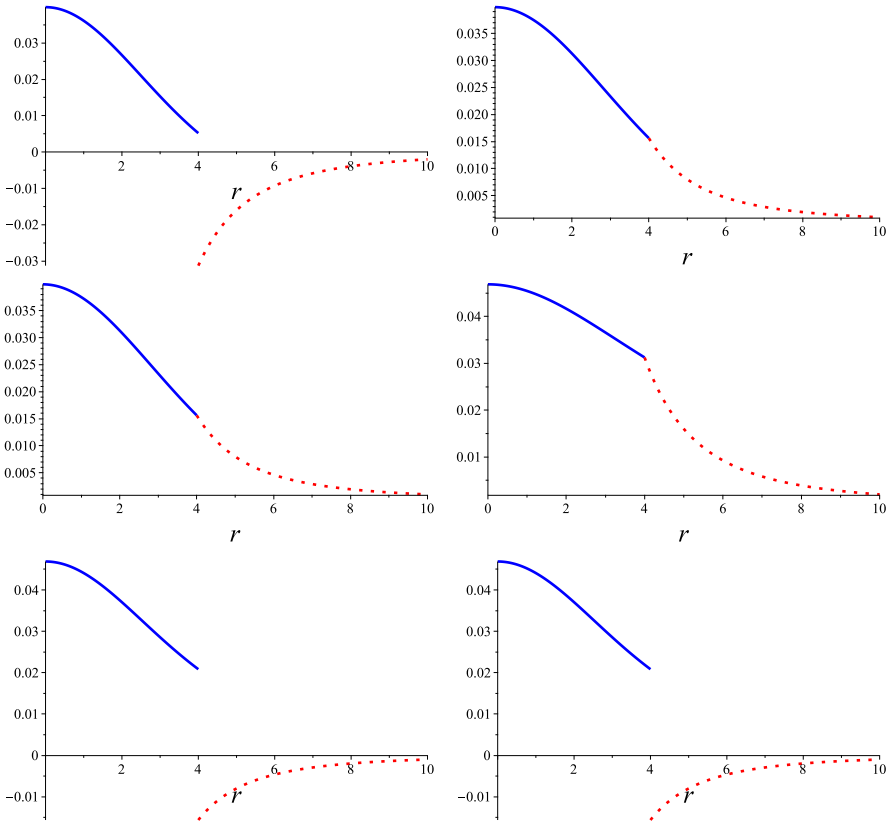

Figure 7.4: The curvature eigenvalues for the interior Buchdahl I metric ($r \leq 4$) and the exterior Schwarzschild metric ($r \geq 4$) for $\kappa = 2$ and $m = 1$.

possible. This seems to indicate that the C^3 procedure is more restrictive than the Darmois approach.

To explain this contradictory result, let us consider the behavior of the thermodynamic variables p and ρ on the matching surface Σ. In all the three cases investigated above, we can see that the pressure vanishes on Σ, but the density is different from zero. In the case of the Tolman III perfect fluid, the density is constant everywhere, even outside the body, and in the case of the Heintzmann II and Buchdahl I solutions, the density vanishes only asymptotically at infinity. It seems that for the Darmois matching approach, this physical obstruction is not a problem. In fact, from a physical point of view, one would expect that pressure and density should vanish outside the object.

On the other hand, the C^3 approach can detect the physical obstruction due to

a non-vanishing density on the matching surface. In fact, in [16], it was shown that in the case of spherically symmetric perfect fluids, the vanishing of the energy-momentum tensor on the matching surface is a necessary condition to perform the matching procedure. This means that the pressure, as well as the density, should vanish on the matching hypersurface. In this sense, from a physical point of view, we can ensure that the C^3 approach is more restrictive than the Darmois approach.

This result also shows that a generalization of Darmois approach would be appropriate to handle the cases in which the jump of the curvature eigenvalues across Σ does not vanish. We will propose such a procedure in the next section.

7.5 C^3 discontinuous matching

The previous results show that the C^3 procedure does not allow to match spherically symmetric perfect fluid spacetimes, whose density and pressure are different from zero on the matching surface.

Now, we will construct a formalism that allows the matching in the case of discontinuities across the matching surface, i.e., $\lambda_n^+ \neq \lambda_n^-$ on Σ for at least one value of n. We will use as a conceptual guide Israel's formalism [23] that allows the existence of discontinuities of the first and second fundamental forms by introducing an effective energy-momentum tensor on the matching surface Σ so that it can be intepreted as a infinitesimal matter shell that join the interior and exterior spacetimes. To this end, let us consider the jump of the eigenvalues across Σ as

$$[\lambda_n] = \lambda_n^- - \lambda_n^+ \,, \tag{7.5.1}$$

In the case of a matching between an interior perfect fluid solution and the exterior Schwarzschild vacuum solution, we have shown that the C^3 procedure implies that ρ and p should be zero on Σ. When these conditions are not satisfied, let us define the surface density σ and pressure π as

$$\sigma = \rho|_\Sigma \,, \qquad P = p|_\Sigma \,. \tag{7.5.2}$$

Then, since in the case of discontinuities we have that $[\lambda_n] \neq 0$, it follows that $\sigma \neq 0$ and $P \neq 0$, in general, as will be shown in concrete examples below. This is equivalent to saying that the explicit values of $[\lambda_n]$ should contain information about σ and P. The question is now whether σ and P can be used to construct a realistic matter shell

on Σ. To this end, consider the jump of the Einstein tensor on Σ, i. e.,

$$[G_{ij}] = G^-_{ij} - G^+_{ij} \,, \quad G^\pm_{ij} = \frac{\partial x^\mu_\pm}{\partial \xi^i}\frac{\partial x^\nu_\pm}{\partial \xi^j} G^\pm_{\mu\nu} \,, \tag{7.5.3}$$

where ξ^i are the coordinates of the surface Σ and $x^\mu_\pm$ are the coordinates of the interior and exterior spacetimes, respectively. Then, $G^\pm_{ij}$ is the Einstein tensor induced on Σ. Furthermore, we introduce an energy-momentum tensor S_{ij} on Σ as

$$[G_{ij}] = kS_{ij} \,. \tag{7.5.4}$$

Certainly, it is always possible to introduce algebraically an energy-momentum tensor in this way. However, the essential point is whether S_{ij} is physically meaningful. To guarantee the fulfillment of this condition, we demand that S_{ij} be induced by the energy-momentum tensors of the interior and exterior spacetimes and be in agreement with their physical significance. Then, in the case of the perfect fluid we are considering here, we demand that

$$S_{ij} = [T_{ij}] = T^-_{ij} - T^+_{ij} = (\sigma + P)u_i u_j + P\gamma_{ij} \,, \tag{7.5.5}$$

where $T^\pm_{ij}$ are the energy-momentum tensors and $\gamma_{ij} = \gamma^\pm_{ij}$ is the metric tensor induced on Σ, respectively.

In summary, in the case of discontinuities, we will say that an interior spacetime can be matched with an exterior one along a boundary shell located on Σ, if there exist a density σ and a pressure P, satisfying the induced Einstein equations (7.5.4) and (7.5.5) and the boundary condition (7.5.2).

To test the above procedure, we consider now the explicit examples presented in the previous sections. First, we notice that in the case of spherical symmetry the coordinates on both sides of the boundary can be chosen as $x^\mu_\pm = (t, r, \theta, \phi)$ and on the matching surface as $\xi^i = (t, \theta, \phi)$. Then, all the components of the quantities $\frac{\partial x^\mu}{\partial \xi^i}$ are constant and the induced tensors can be calculated in a straightforward way.

Tolman III

In this case, from the results presented in Sec. 7.4.1, we obtain for the jump of the eigenvalues along the matching surface $r = K$ the following expressions

$$[\lambda_2] = [\lambda_3] = [\lambda_4] = 0 \,, \quad [\lambda_1] = [\lambda_5] = [\lambda_6] = \frac{3m}{K^3} = 4\pi\sigma \,, \tag{7.5.6}$$

which agrees with the result that on the matching surface the pressure vanishes. Furthermore, the jump of components of the induced Einstein tensor can be expressed as

$$[G_{tt}] = \frac{4mr^2 + K^3 - K^3 f^2(r)}{K^3 r^2}\gamma_{tt} \,, \tag{7.5.7}$$

$$[G_{\theta\theta}] = \frac{6mr^2}{K^3}\,\frac{f(K) - f(r)}{3f(K) - f(r)} \,, \quad [G_{\phi\phi}] = \sin^2\theta\,[G_{\theta\theta}] \,. \tag{7.5.8}$$

It is then easy to see that on the matching surface $r = K$, the induced Einstein equations for dust are satisfied

$$[G_{ij}] = k\sigma u_i u_j \,, \quad u^i = (-1, 0, 0) \,, \tag{7.5.9}$$

proving that, in fact, a realistic dust shell can be introduced that allows us to match, in the framework of the C^3 matching procedure, the interior Tolman III solution with the exterior Schwarzschild spacetime.

An explicit calculation gives

$$[G_{tt}] = \frac{6m}{K^3} \,, \tag{7.5.10}$$

$$[G_{\theta\theta}] = [G_{\phi\phi}] = 0. \tag{7.5.11}$$

Heintzmann II

In this case, from the results presented in Sec. 7.4.2, we obtain for the jump of the eigenvalues along the matching surface $r = r_0$ the following expressions

$$[\lambda_2] = [\lambda_3] = [\lambda_4] = 0 \,, \quad [\lambda_1] = [\lambda_5] = [\lambda_6] = \frac{(14m - 9r_0)m}{3r_0^3(m - r_0)} = 4\pi\sigma \,. \tag{7.5.12}$$

From the expressions for the induced Einstein tensor, we obtain the jump

$$[G_{tt}] = \frac{2(14m - 9r_0)m}{3r_0^3(m - r_0)} \,, \tag{7.5.13}$$

$$[G_{\theta\theta}] = [G_{\phi\phi}] = 0 \,. \tag{7.5.14}$$

In this case, the induced Einstein equations $[G_{ij}] = k\sigma u_i u_j$ are satisfied for

$$\sigma = \frac{(14m - 9r_0)m}{12\pi r_0^3(m - r_0)} \,, \quad u^i = (-1, 0, 0) \,, \tag{7.5.15}$$

an expression that fulfills the compatibility condition (7.5.2).

Buchdahl I

From the results presented in Sec. 7.4.3, we obtain the following jumps for the eigenvalues along the surface $r = 2\kappa m$

$$[\lambda_2] = [\lambda_3] = [\lambda_4] = 0\,, \quad [\lambda_1] = [\lambda_5] = [\lambda_6] = \frac{9\kappa - 4}{24\kappa^4 m^2} = 4\pi\sigma\,. \tag{7.5.16}$$

Furthermore, the jump of the induced Einstein tensor reads

$$[G_{tt}] = \frac{9\kappa - 4}{12\kappa^4 m^2}\,, \tag{7.5.17}$$

$$[G_{\theta\theta}] = [G_{\phi\phi}] = 0\,. \tag{7.5.18}$$

Then, the induced Einstein equations $[G_{ij}] = k\sigma u_i u_j$ are satisfied for

$$\sigma = \frac{9\kappa - 4}{96\pi\kappa^4 m^2}\,, \quad u^i = (-1, 0, 0)\,, \tag{7.5.19}$$

in accordance with the compatibility condition (7.5.2).

Notice that in all the above examples the energy-momentum tensor of the dust shell can be expressed as

$$S_{ij} = \frac{k}{4\pi}[\lambda_1] u_i u_j\,, \tag{7.5.20}$$

indicating that the properties of the boundary shell are determined in an invariant manner by the curvature eigenvalues.

7.6 Discussion and remarks

In this work, we have analyzed the problem of matching exact solutions of Einstein equations in order to describe a spacetime completely. We limit ourselves to the case of spherically symmetric solutions of Einstein equations. Since the vacuum Schwarzschild solution is singular at the origin of coordinates, it is believed that an appropriate non-vacuum and singularity-free solution can be used to "cover" the Schwarzschild singularity in such a way that the entire spacetime is regular. This is how one expects that classical general relativity can get rid of curvature singularities. This seems to be a simple method to solve such an important problem of general relativity. However, the problem arises of matching the non-vacuum and vacuum

solutions in such a way that the entire differential manifold is well behaved. This is why the matching problem is very important in general relativity.

We have applied the Darmois and the C^3 approaches to three different perfect solutions of Einstein equations, which could be considered as appropriate interior candidates to be matched with the exterior Schwarzschild solution. These are the Tolman III, Heintzmann II, and Buchdahl I solutions. We have shown that the mentioned matching procedures lead to contradictory results. According to Darmois approach, all the three candidates satisfy the matching conditions and can be interpreted as interior counterparts of the exterior Schwarzschild metric. However, the C^3 approach shows that none of the three solutions satisfy the C^3 matching conditions. We explain this contradictory result by noticing that in all three perfect fluid solutions, the energy density shows a discontinuity across the matching surface. Although this is not an obstacle for the Darmois procedure, the C^3 approach demands that the pressure and the density as well vanish on the matching surface. This is why both approaches lead to different results. We mention that we obtained the same result in the case of the Durgapal IV and V spacetimes [9], which are spherically symmetric perfect fluid solutions of Einstein equations.

To handle the case in which discontinuities are present along the matching surface Σ, we propose in this work a generalization of the C^3 matching procedure. It consists essentially on demanding that the 3-dimensional hypersurface Σ be also described by a solution of Einstein equations. In fact, we consider the induced Einstein tensor on Σ and show that it can be represented as a realistic energy-momentum tensor that describes the matter inside a boundary shell located on Σ. In the cases considered in this work, it turned out that the boundary corresponds to a dust shell. For more general interior solutions, we expect to obtain shells with more intricate internal structures.

8 Gravitational field of black holes surrounded by dark matter with anisotropic pressure

8.1 Introduction

The common disk-like particle flow lying around compact objects, dubbed accretion disk, permits the direct observation of the radiation emitted by the orbiting material rotating in the gravitational field of an astronomical object. In particular, the corresponding spectra are commonly observed and so, as the accreting material fuels the region around the central object, observers can extract information about properties of the whole system. For extreme compact objects the relativistic effects are clearly non-negligible. On one side, the luminosity itself can be described simply by some emission spectrum model, however, on the other side, the motion of particles in the disk and the trajectory of light rays escaping the disk require Einstein's field equations. Thus, the exterior geometry of the accretor, namely the central object, can be modeled through a metric with a given symmetry which will determine the properties of the observed radiation. In this picture, one can investigate black holes, white dwarfs, neutron stars, quasars, radio galaxies, X-ray binaries, but also more exotic, hypothetical objects, e.g. boson stars or gravastars.

The central object's mass grows through accretion and to fully describe the disks, one requires an exterior configuration and then solves the hydrodynamic equilibrium equations. Frequently, "exotic" matter contributions seem to be needed to describe hypothetical objects that are massive and compact, in order to fulfill stability criteria. Analogous examples can often be found in the case of wormholes and for cosmological backgrounds.

In this work, we consider a static spherically symmetric configuration composed of a central black hole surrounded by a dark matter envelope. The gravitational field in the vacuum region around the black hole is described by the exterior Schwarzschild space-time while the corresponding dark matter distribution, located at a given dis-

tance from the black hole, and its properties, is described by making use of the Tolman-Oppenheimer-Volkoff (TOV) equations.

We assume that the dark matter envelope does not interact with the baryonic matter of the accretion disk that is located within the envelope itself. We then apply the theory of black hole accretion developed in Ref. [35] for astrophysical black hole candidates, in order to model the emitted spectrum from the accretion disk. In particular, we aim to test the consequences of two main assumptions: (i) dark matter in endowed with a non-vanishing radial pressure term entering the TOV equations, namely $P_r(r) = P(r)$ and (ii) second, we assume the energy momentum tensor to be anisotropic, leading to an additional pressure term, which is interpreted as a non vanishing tangential pressure, $P_\theta(r)$. We physically motivate these two choices and characterize the dark matter distribution accordingly, by computing the difference $P_\theta(r) - P(r)$.

It should be stressed that the theory of anisotropic fluids is well known in the literature. In particular, it was shown that anisotropic fluids may be geodesic in general relativity in Ref. [20]. A general study of spherically symmetric dissipative anisotropic fluids is given in Ref. [**?**]. Exact static spherically symmetric anisotropic solutions of the field equations are obtained and analyzed in Refs. [**? ?**]. Anisotropic stars in general relativity and their mass-radius relations are computed in Ref. [**?**]. In this work we instead study the effects of dark matter with anisotropic pressures on test particles in the accretion disk present within the dark matter and the spectra of the disk. In particular we compare the motion of particles and accretion disk's spectra with the cases of isotropic dark matter and a Schwarzschild black hole in vacuum.

The chapter is organized as follows: in Sect. 8.2, we describe a configuration that consists of a black hole surrounded by a dark matter distribution. We then introduce the static line element with anisotropic energy momentum tensor containing tangential pressure P_θ used to describe the dark matter envelope. Afterwards, we review the definitions of flux, differential luminosity, and spectral luminosity as presented in the Novikov-Page-Thorne (NPT) model. In Sect. 8.3, we solve the Tolman-Oppenheimer-Volkoff (TOV) equations and calculate the metric functions fulfilling boundary conditions in the different regions of the space-time. Then we compute the angular velocity, energy, and angular momentum of the configuration and plot the modeled flux and luminosity spectrum for various values of the parameter related to the dark matter anisotropy. Implications of the model for astrophysical black hole candidates are then discussed in in Sect. 8.4.

8.2 Black hole surrounded by anisotropic dark matter

In the following we investigate a system composed of a static black hole with a dark matter envelope around it, where the dark matter is introduced *only* with the purpose of modifying the geometry around the black hole. Since the black hole represents the accretor, one can split the mass profile of the overall configuration into three regions,

$$M(r) = \begin{cases} M_{BH}, & r_g < r \leq r_b, \\ M_{BH} + M_{DM}(r), & r_b \leq r \leq r_s, \\ M_{BH} + M_{DM}(r_s), & r_s \leq r, \end{cases} \tag{8.2.1}$$

where $r_g = 2M_{BH}$ is the gravitational radius and M_{BH} is the mass black hole, whereas r_b and r_s are the inner and outer edges (radii) of the dark matter envelope. In particular, r_b corresponds to the boundary that separates the inner vacuum region from the outer distribution of dark matter. Accordingly, the above configuration can be described as follows:

- the core is modeled by the accretor in the form of a black hole. Its mass, M_{BH}, is a free parameter of our model;
- the black hole is surrounded by a dark matter shell that extends from a radius r_b up to the radius r_s;
- at r_s, the dark matter mass reaches its maximum value $M_{DM}(r_s)$ and beyond r_s we assume vacuum;
- at $r \geq r_s$ the total mass of the system is defined as $M_T = M(r_s)$.

To model the dark matter distribution in the shell $r \in [r_b, r_s]$, we assume an exponential sphere profile of the form

$$\rho(r) = \rho_0 e^{-\frac{r}{r_0}}, \quad r \geq r_b, \tag{8.2.2}$$

where ρ_0 is the dark matter density at $r = 0$ and r_0 is the scale radius. The exponential density profile was introduced in Ref. [**?**] to explain the rotation curve in the bulge of the Milky Way Galaxy. Indeed it showed a better fit of the observational data with respect to the widely adopted de Vaucouleurs law in the inner part of the galaxy. Recently it was also applied to study the effects of non-vanishing dark matter pressure in the entire Milky Way Galaxy [**?**].

As a consequence, assuming spherical symmetry, the dark matter mass profile is given by

$$M_{DM}(r) = \int_{r_b}^{r} 4\pi\tilde{r}^2\rho(\tilde{r})\,d\tilde{r}, \tag{8.2.3}$$

which yields

$$M_{DM}(x) = 8\pi r_0^3\rho_0\left[e^{-x_b}\left(1+x_b+\frac{x_b^2}{2}\right)-e^{-x}\left(1+x+\frac{x^2}{2}\right)\right], \tag{8.2.4}$$

for $r > r_b$, where we have substituted $x = r/r_0$ and $x_b = r_b/r_0$. For vanishing r_b, the profile (8.2.3) reduces to the one obtained in [**?**].

8.2.1 TOV equations with anisotropic pressure

To describe the physical properties of the system in Eq. (8.2.1), we consider the spherical symmetric line element

$$ds^2 = e^{N(r)}dt^2 - e^{\Lambda(r)}dr^2 - r^2\left(d\theta^2+\sin^2\theta d\varphi^2\right), \tag{8.2.5}$$

where, as usual, we take (t, r, θ, φ) as time and spherical coordinates, respectively, while $N(r)$ and $\Lambda(r)$ represent the unknown metric functions.

The energy-momentum tensor is given by

$$T^{\alpha\beta} = (\rho + P_\theta)u^\alpha u^\beta - P_\theta g^{\alpha\beta} + (P - P_\theta)\chi^\alpha\chi^\beta\,, \tag{8.2.6}$$

where $u^\alpha u_\alpha = 1 = -\chi^\alpha\chi_\alpha$, $u^\alpha\chi_\alpha = 0$, $u^\alpha = e^{-N/2}\delta_0^\alpha$ is the four-velocity and $\chi^\alpha = e^{-\Lambda/2}\delta_1^\alpha$ is a unit space-like vector in the radial direction, with δ_i^α the Kronecker symbol [**?**]. Using Einstein's equations for the line element (8.2.5) and the energy-momentum tensor(8.2.6) we obtain the following expressions [**?**]

$$\begin{aligned}\frac{dP(r)}{dr} &= -(\rho(r)+P(r))\frac{M(r)+4\pi r^3P(r)}{r(r-2M(r))} \\ &\quad +\frac{2}{r}\left(P_\theta(r)-P(r)\right),\end{aligned} \tag{8.2.7}$$

$$\frac{dN(r)}{dr} = 2\,\frac{M(r)+4\pi r^3P(r)}{r(r-2M(r))}, \tag{8.2.8}$$

which generalize the TOV equations to the case of anisotropic pressures and relate the density, $\rho(r)$, with the radial pressure, $P(r)$, and the tangential term, $P_\theta(r)$. In general this is a system of two equations in four unknown, and therefore two functions must be provided in order to close it. Typically this is done by specifying the equations of state that relate the pressures $P_\theta(r)$ and $P(r)$ to the density. In our model, however, $\rho(r)$ is the dark matter density given by Eq. (8.2.2), whereas $M(r)$ is given by Eq. (8.2.1); and therefore, these quantities are no longer unknown functions to be determined. Notice, however, that one unknown function remains to be specified. This function can be taken to be the pressure difference $P_\theta(r) - P(r)$, appearing in Eq. (8.2.7), which is not known *a priori*.

A possible viable strategy to employ has been discussed in Ref. [**?** **?**], where the *anisotropy function*, $\Delta(r)$, has been introduced as

$$\Delta(r) \equiv P_\theta(r) - P(r) = \alpha\mu(r)P(r)\,, \tag{8.2.9}$$

where α is a free constant, physically interpreted as the anisotropy parameter, while μ is the *compactness* of the system defined by

$$\mu(r) = \frac{2M(r)}{r} = 1 - e^{-\Lambda(r)}\,. \tag{8.2.10}$$

In general, μ indicates the strength of the gravitational field. If $\mu \ll 1$ the field is weak, if $\mu \sim 1$ the field is strong. An interesting characteristics of Eq. (8.2.9) is that μ guarantees the required vanishing of the anisotropy of pressures at $r = 0$ (notice that typically $M(r) \sim r^3$ close to the center). Moreover in the weak field limit the anisotropy of pressure is not expected to be important. In addition, this anzatz makes sure that the tangential pressure vanishes at the surface of the object [**?**], in our case at the surface of dark matter envelope.

Notice that according to Eq. (8.2.9), $\alpha < 0$ corresponds to $P_\theta < P$, $\alpha = 0$ corresponds to the isotropic case $P_\theta = P$ and $\alpha > 0$ corresponds to $P_\theta > P$. The case of a static black hole surrounded by a dark matter envelope with isotropic pressures, i.e. $\alpha = 0$, has been studied in detail by some of us in Ref. [**?**] within a model that closely follows the one considered here.

Furthermore, to analyze our model, we should now establish the boundary conditions between inner and outer solutions.

8.2.2 Boundary conditions

As stated above, the innermost region is given by a black hole vacuum solution with the event horizon located at $r = r_g$, while the exterior region corresponds to the dark matter distribution extending from a radius $r_b > r_g$ to an outer radius $r_s > r_b$. The values of density, pressures and metric functions at the boundary are determined from $\rho(r_b), P(r_b)$ and $N(r_b)$. They can be computed immediately, obtaining

$$\rho(r_b) = \rho_b = \rho_0 \, e^{-\frac{r_b}{r_0}}, \tag{8.2.11}$$

$$P(r_b) = P_b, \tag{8.2.12}$$

$$N(r_b) = N_b = \ln\left(1 - \frac{r_g}{r_b}\right). \tag{8.2.13}$$

Consequently, the unknown metric functions, $N(r)$ and $\Lambda(r)$, are evaluated as

$$e^{N(r)} = \begin{cases} 1 - \dfrac{r_g}{r}, & r_g < r \leq r_b, \\ e^{N_r(r)}, & r_b \leq r \leq r_s, \\ 1 - \dfrac{2M(r_s)}{r}, & r_s \leq r, \end{cases} \tag{8.2.14}$$

and

$$e^{\Lambda(r)} = \begin{cases} \left(1 - \dfrac{r_g}{r}\right)^{-1}, & r_g < r \leq r_b, \\ \left(1 - \dfrac{2M(r)}{r}\right)^{-1}, & r_b \leq r \leq r_s, \\ \left(1 - \dfrac{2M(r_s)}{r}\right)^{-1}, & r_s \leq r. \end{cases} \tag{8.2.15}$$

where $N_r(r)$ is simply function $N(r)$ in the interval $r \in [r_b, r_s]$ which must be numerically evaluated from the TOV equations fulfilling the corresponding boundary conditions.

It is worth noticing that if we follow this consolidate procedure for matching different spacetimes by imposing continuity of the first and second fundamental forms, the dark matter pressure should vanish when $r = r_b$. Therefore the condition $P(r_b) = P_b$ leads to a non-continuous matching, since the first derivatives of the metric show a jump at the boundary. However, there is a natural physical explanation for the discontinuity. The common interpretation is to assume the presence of a massive surface

layer at r_b for which the three dimensional energy momentum can be evaluated from the matching conditions, as discussed in Refs. [**? ?**].

8.2.3 Radiative flux and spectral luminosity

Bearing in mind the above results, we can now investigate the flux and spectral luminosity produced by an accretion disk in the geometry with the above proposed ansatz. The disk extends from an inner edge r_i which is usually taken as the innermost stable circular orbit (ISCO) for test particles, $r_i = r_{ISCO}$. To this end, we follow the simple approach proposed by Novikov-Thorne and Page-Thorne in Refs. [35**?**] and write the radiative flux $\mathcal{F}$ as

$$\mathcal{F}(r) = -\frac{\dot{m}}{4\pi\sqrt{g}}\frac{\Omega_{,r}}{(E-\Omega L)^2}\int_{r_i}^{r}(E-\Omega L)\,L_{,\tilde{r}}d\tilde{r}. \tag{8.2.16}$$

The above quantity depends upon $\dot{m}$, i.e., the disk mass accretion rate, which is unknown. In the simplest case, we can take it as constant and we can set $\dot{m} = 1$, which is equivalent to considering the normalized flux per unit accretion rate, i.e., $\mathcal{F}(r)/\dot{m}$. Moreover, g is the determinant of the three-dimensional subspace with coordinates (t, r, φ) and is given by $\sqrt{g} = \sqrt{g_{tt}g_{rr}g_{\varphi\varphi}}$. The quantities appearing in Eq. (8.2.16) are,

$$\Omega(r) = \frac{d\varphi}{dt} = \sqrt{-\frac{\partial_r g_{tt}}{\partial_r g_{\varphi\varphi}}}, \tag{8.2.17}$$

$$E(r) = u_t = u^t g_{tt}, \tag{8.2.18}$$

$$L(r) = -u_\varphi = -u^\varphi g_{\varphi\varphi} = -\Omega u^t g_{\varphi\varphi}, \tag{8.2.19}$$

$$u^t(r) = \dot{t} = \frac{1}{\sqrt{g_{tt}+\Omega^2 g_{\varphi\varphi}}}, \tag{8.2.20}$$

namely $\Omega = \Omega(r)$ is the orbital angular velocity, $E = E(r)$ is the energy per unit mass and $L = L(r)$ is the orbital angular momentum per unit mass of the test particle. Additionally, ∂_r is the derivative with respect to the radial coordinate r, a dot represents the derivative with respect to the proper time and u^t is the time component of the 4-velocity.

Another important quantity is the differential luminosity that is interpreted as the energy per unit of time reaching an observer at infinity. We denote it by $\mathcal{L}_\infty$ and

estimate it through the flux, $\mathcal{F}$, by means of the following relation [35**?**]

$$\frac{d\mathcal{L}_\infty}{d\ln r} = 4\pi r\sqrt{g}E\mathcal{F}(r). \tag{8.2.21}$$

If the radiation emission is assumed to be well described by that of a black body, then we can express the spectral luminosity at infinity $\mathcal{L}_{\nu,\infty}$ as a function of the radiation's frequency ν as [**?**]

$$\nu\mathcal{L}_{\nu,\infty} = \frac{60}{\pi^3}\int_{r_i}^{\infty}\frac{\sqrt{g}E}{M_T^2}\frac{(u^t y)^4}{\exp\left[u^t y/\mathcal{F}^{*1/4}\right]-1}dr, \tag{8.2.22}$$

where $y = h\nu/kT_*$, h is the Planck constant, k is Boltzmann's constant, M_T is the total mass, $\mathcal{F}^* = M_T^2\mathcal{F}$ and we have taken $r_i = r_{ISCO}$. Also, T_* is the characteristic temperature defined from the Stefan-Boltzmann law, which reads

$$\sigma T_* = \frac{\dot{m}}{4\pi M_T^2}\,, \tag{8.2.23}$$

with σ the Stefan-Boltzmann constant.

To compare with a Schwarzschild black hole in vacuum it is also interesting to calculate the radiative efficiency of the source, i.e. the amount of rest mass energy of the disk that is converted into radiation which is given by

$$\mathcal{L}_\infty/\dot{m} = 1 - E(r_{ISCO}), \tag{8.2.24}$$

that in the case of Schwarzschild gives the known result $\eta = (1 - E(r_{ISCO}))\times 100\% \simeq 5.7\%$.

In Fig. 8.1 we show schematic representation of the system examined here. Left panel presents two dimensional diagram of the equatorial plane of the system, whereas right panel shows a cross section of the three dimensional diagram. One can see that $r_b < r_{ISCO} < 3r_g$. Thus the presence of dark matter alters the geometry around a black hole and decreases the value of r_{ISCO}.

8.3 Discussion of numerical results

To compute orbital parameters of test particles, flux, differential and spectral luminosities of an accretion disk, we need first to numerically solve the TOV equations. The corresponding numerical solutions for the pressure and the metric functions

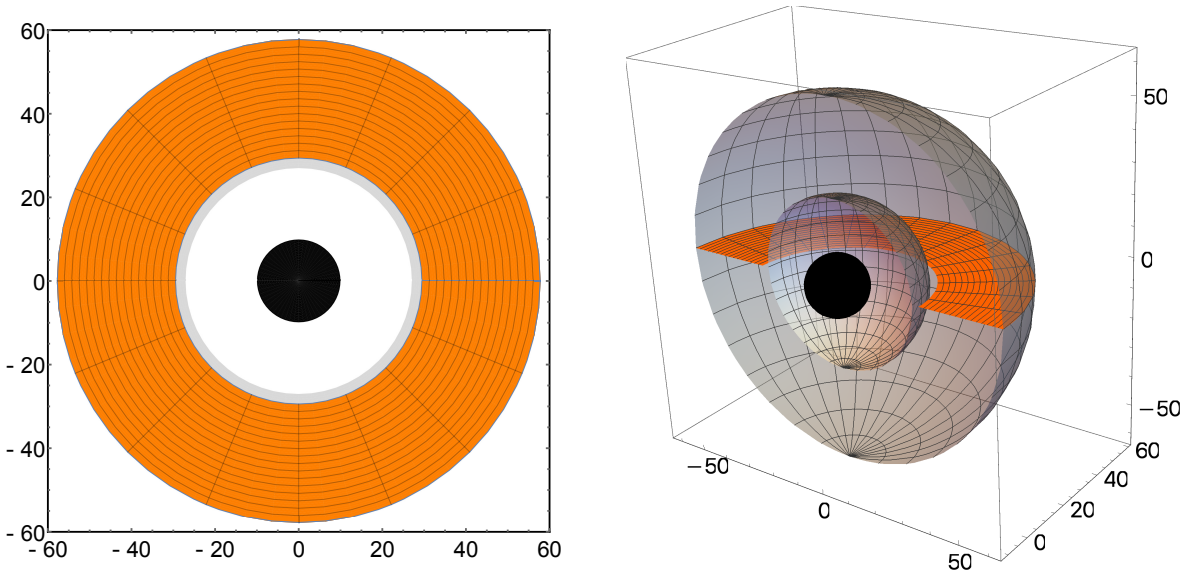

Figure 8.1: Left panel: two dimensional schematic illustration of the system at the equatorial plane. The central black disk represents a black hole of radius $r_g = 2M_{BH} = 10^9 M_\odot \approx 9.866$ AU, the gray disk shows dark matter distribution starting from $r_b = 27.133$ AU up to $r_s = 57.755$ AU, the orange disk represents an accretion disk of inner radius $r_{ISCO} = 29.414$ AU and outer radius r_s. Right panel: the cross section of the three dimensional plot. The black sphere is the black hole, the dark matter distribution is confined within the two gray spheres of radii r_b and r_s, the accretion disk is at the equatorial plane

.

must fulfill the boundary conditions above reported in Eqs. (8.2.14)-(8.2.15). In particular, holding $P(r) = 0$ at $r = r_s$, i.e. at the surface radius of the dark matter envelope, implies that N and Λ have to ensure $N(r_s) = -\Lambda(r_s)$ on the surface. However, the numerical value of function $N(r)$ which denote as $N_n(r_s)$, obtained from the numerical solution of the TOV equations, is not equal to $-\Lambda(r_s)$. This is related to the fact that the boundary condition $N(r_b) = \ln(1 - r_g/r_b)$ is imposed while solving the TOV equations, whereas the boundary condition $N(r_s) = \ln(1 - 2M(r_s)/r_s)$ is not. Therefore in order to satisfy the latter boundary condition one needs a redefinition of function N_n. The most suitable redefinition of N_n is the following

$$N_r(r) = N_n(r) - \left[N_n(r_s) - \ln\left(1 - \frac{2M(r_s)}{r_s}\right)\right]\frac{r - r_b}{r_s - r_b}, \tag{8.3.1}$$

which clearly fulfills the boundary conditions in Eq. (8.2.14).

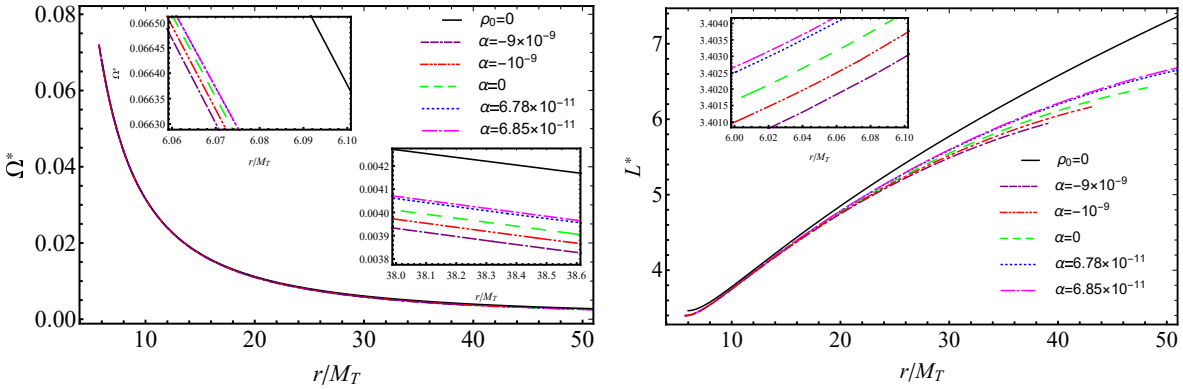

Figure 8.2: Left panel: numerical evaluation of the orbital angular velocity Ω^* of test particles in the accretion disk around a static black hole of mass $M_{BH} = 5 \times 10^8 M_\odot \approx 4.933 AU$ in the presence of anisotropic dark matter as a function of r/M_T. Right panel: numerical evaluation of orbital angular momentum L^* of test particles in the accretion disk as a function of r/M_T. In both figures the solid black curves represents the case of a static black hole without dark matter while the other curves represent anisotropic dark matter envelopes with $\rho_0 = 0.85 \times 10^{-5} AU^{-2}$

.

The numerical analysis that follows shows the effects of the presence of the dark matter envelope as depending on the value of the parameter α in Eq. (8.2.9). It is worth noticing that in order to solve the TOV equations one needs to restrict α to negative or small positive values. The outer boundary of the envelope r_s is determined from the TOV equations by imposing $P(r_s) = 0$, once ρ_0, P_b and α are fixed. Finally the total amount of dark matter in the envelope is given by $M_{DM}(r_s)$.

With these ingredients we fully determine the metric functions and therefore we can study the motion of test particles within the dark matter cloud under the hypothesis that dark matter doesn't interact with the baryonic matter of the accretion disk and therefore test particles move on geodesics in the geometry produced by the dark matter envelope surrounding the black hole. The value of r_{ISCO} is obtained from the evaluation of stable circular orbits within the dark matter envelope and it is set as the inner edge of the disk.

Comparison of the values of r_s, M_{DM} and r_{ISCO} for different values of α can be found in Tab. 8.1.

It is worth noticing that, for a fixed value of ρ_0 and P_b the TOV equations can be solved for a wide range of values of $\alpha < 0$, which implies $P_\theta < P$. On the other

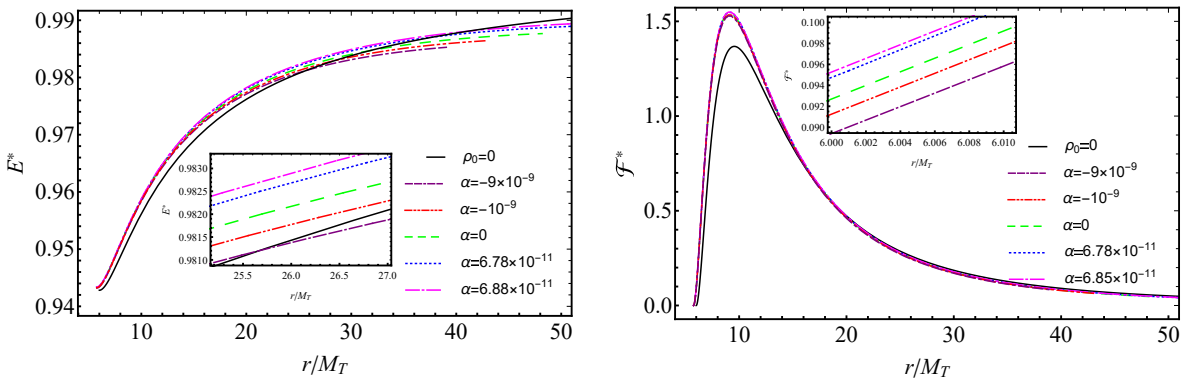

Figure 8.3: Left panel: numerical evaluation of energies E^* of test particles in the accretion disk around a static black hole of mass $M_{BH} = 5 \times 10^8 M_\odot \approx 4.933 AU$ in the presence of anisotropic dark matter as a function of r/M_T. Right panel: numerical evaluation of the flux $\mathcal{F}$ divided by 10^{-5} of the accretion disk as a function of r/M_T. In both figures the solid black curves represents the case of a static black hole without dark matter while the other curves represent anisotropic dark matter envelopes with $\rho_0 = 0.85 \times 10^{-5} AU^{-2}$.

hand, for $\alpha > 0$, i.e. $P_\theta > P$ there are maxima of α for which the TOV equations lead to unstable dark matter configurations and the TOV equations will not have solutions. Also the total dark matter mass tends to reach a maximum value of $M_{DM}(r_s) \simeq 2.12342 \times 10^{-2}\, M_{BH}$ for $\alpha \simeq -10^{-8} \div 10^{-9}$. Similarly, considering a central black hole of mass $M_{BH} = 5 \times 10^8 M_\odot \approx 4.933 AU$ (with $M_\odot$ being the mass of the Sun) the value of α affects only slightly the location of the ISCO, while it affects significantly the outer edge of the envelope r_s i.e. r_s and $M_{DM}(r_s)$ increase with increasing α from negative to positive values. On the contrary, the radiative efficiency of the accretion disk decreases as α increases. See for Tab. 8.1 details.

With the above numerical setup, in Fig. 8.2 we plot $\Omega^\star = M_T \Omega$ and $L^\star = L/M_T$, i.e. the dimensionless orbital angular velocity and orbital angular momentum of test particles in the presence of a dark matter envelope, as functions of r/M_T. The solid curves represent the case of a static black hole without dark matter, namely $\rho_0 = 0$, and are easily distinguished from the other curves. For other curves the values of density and pressure are fixed as $\rho_0 = 0.85 \times 10^{-5} AU^{-2}$ and $P_b = 2.356 \times 10^{-8} AU^{-2}$, and α is varied. In particular the distinction is more marked for orbital angular momentum $L^\star$, especially for large values of r/M_T.

Similar plots for $E^\star$ and $\mathcal{F}^\star$, namely the energy per unit mass of test particles and the disk's flux, are obtained in Fig. 8.3. In the case of energy one can see that for

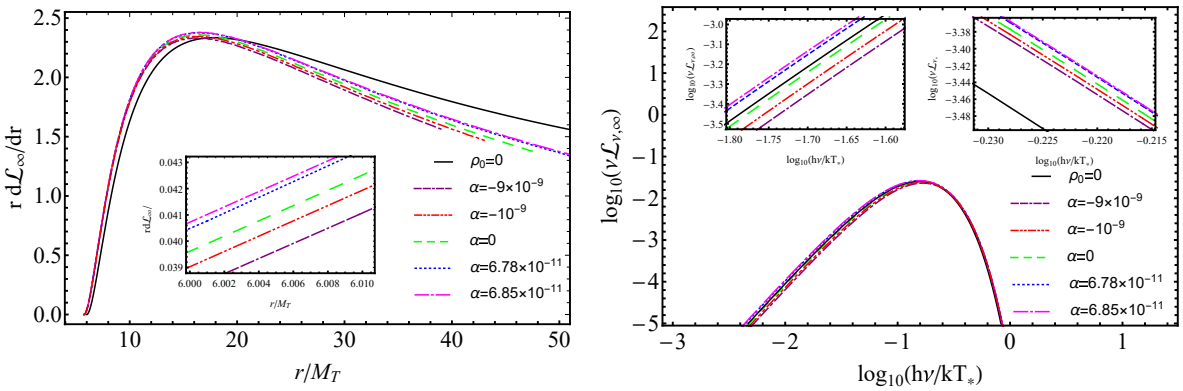

Figure 8.4: Left panel: numerical evaluation of the differential luminosity of the accretion disk scaled in powers of 10^{-2} as a function of r/M_T. Right panel: numerical evaluation of the spectral luminosity of the accretion disk as a function of $h\nu/kT_*$, i.e. as a function of frequency. In both figures the solid curves represents the case of a static black hole without dark matter. The intersection points are listed in Table 8.2.

smaller r/M_T $E^\star$ is larger than the pure vacuum case while it becomes smaller r/M_T increases. Consequently, for each α there is an intersection point of the $\rho_0 = 0$ curve with the $\rho_0 = 0.85 \times 10^{-5} AU^{-2}$ curve which produce the same energy. In the case of flux, it is noticeable that the presence of anisotropic dark matter with different α increases the maximum with respect to $\rho_0 = 0$ case.

The differential luminosity as a function of r/M_T is reported in the left panel of Fig. 8.4. The numerical evaluation is scaled in powers of 10^{-2} and shows how the absence of dark matter produces smaller luminosity with respect to the case with dark matter for small radii up to $r/M_T \simeq 15$, and larger luminosity for larger values of r/M_T. This suggests that the accretion disk in the presence of dark matter should emit more energy with respect to the accretion disk in vacuum for large frequencies, as it can be seen from the right panel of Fig. 8.4 which shows the spectral luminosity of the accretion disk as a function of the radiation frequency in a log-log plot. In fact, all frequency ranges for $\alpha > 0$ posses larger luminosity with respect to the $\rho_0 = 0$ case, i.e. Schwarzschild. However for $\alpha \leq 0$ the situation is different and at lower frequencies the luminosity is lower and at higher frequencies the luminosity higher than the Schwarzschild case.

It is relevant to notice that, although our approach is model-dependent since it relies on the assumptions made on compactness, see Eq. (8.2.9), the various possible values of α do not impact significantly on the physics of the disk's emission. This can be seen from the fact that the cases with anisotropic pressures are similar to each

other and to the isotropic case, i.e. $\alpha = 0$, when compared with the vacuum case (solid line in the plots), suggesting that the effects on the spectrum are due mostly to the presence of dark matter rather than to the possible anisotropies.

From an experimental perspective, in principle, it would be possible to obtain information about the presence of dark matter from the spectra of accretion disks, if the other relevant quantities, such as the black hole mass and the disk's ISCO can be determined independently. Last but not least, it is important to remember that even the observable properties of the dark matter distribution are also model dependent, since they rely on the choice made in Eq. (8.2.2). Although the choices of different density profiles in Eq. (8.2.2), equations of state and prescriptions for the anisotropies in Eq. (8.2.9) would modify the values of quantities such as r_{ISCO} and the flux of the accretion disk, we may expect that the overall qualitative features due to the presence of dark matter would remain unchanged.

The case when $\alpha = 0$, or $P_\theta = P$, has been considered in [**?**]. In principle, one can expect that tangential pressures alone, i.e. in the absence of the radial pressures, also known as 'Einstein cluster' [**? ? ?**], could also reproduce analogous results providing *de facto* a degeneracy between the different approaches. The case of vanishing radial pressures is interesting in itself as it may approximate a rotating fluid while keeping the advantage of making the equations much easier and it has been used to model the properties of dark matter halos in [**?**]. The observational features of accretion disks in the Einstein cluster will appear in a separate article [**?**].

For the sake of clarity, in Fig. 8.5 we show the difference in luminosity between the $\rho_0 = 0$ (Schwarzschild) case and the cases with different values of α (with fixed $\rho_0 = 0.85 \times 10^{-5} AU^{-2}$ and $P_b = 2.356 \times 10^{-8} AU^{-2}$). The intersection points indicate that there exist frequencies for which the $\rho_0 \neq 0$ case with various α can mimic the Schwarzschild case. However the overall spectrum for the cases in the presence of dark matter differs from that of the Schwarzschild case and the deviation, which appears to be larger at smaller frequencies, may help to constrain the values of α and ρ_0 from observations.

In Table 8.2 we show numerical values of the intersection points illustrated in Fig. 8.5. For fixed $\rho_0 = 0.85 \times 10^{-5} AU^{-2}$ and $P_b = 2.356 \times 10^{-8} AU^{-2}$ and increasing values of α the difference in luminosity decrease and so does the frequency. These numbers show the frequency at which the disk surrounding a Schwarzschild black hole in vacuum can be mimicked by that of a black hole surrounded by dark matter with a given value of α.

Finally in Fig. 8.6 we plot the efficiency of the source as a function of α for different densities $\rho_0^* = 0.85$, 0.80 and 0.75, where $\rho_0^* = \rho_0/(10^{-5} AU^{-2})$. It is evident that

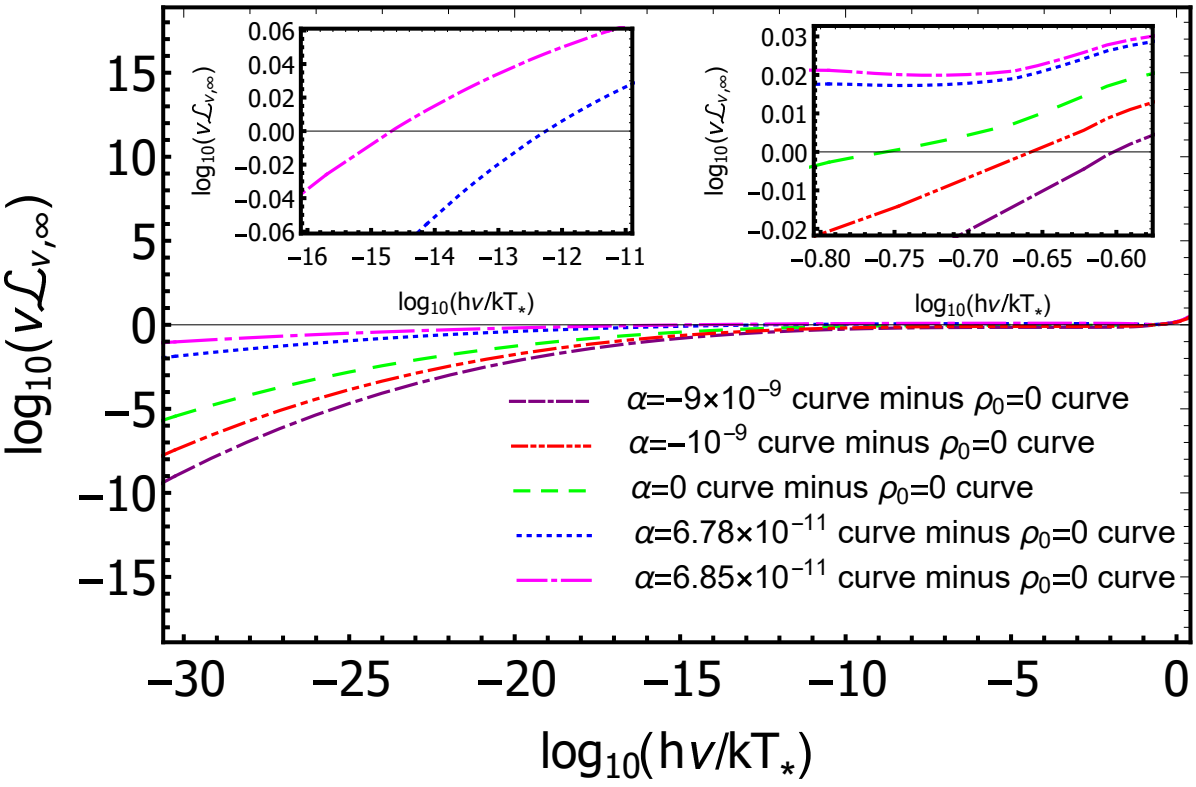

Figure 8.5: The difference of spectral luminosity of the accretion disk between different α curves (with fixed $\rho_0 = 0.85 \times 10^{-5} AU^{-2}$ and $P_b = 2.356 \times 10^{-8} AU^{-2}$) and the vacuum case, i.e. $\rho_0 = 0$.

negative α will yield larger efficiency with respect to the Schwarzschild black hole in vacuum (5.72%) and for positive α the efficiency will be slightly smaller than 5.72%. For numerical values of the efficiency see Table 8.1.

8.4 Final outlooks

We considered a spherically symmetric configuration composed of a central black hole surrounded by a spherical dark matter envelope with anisotropic pressures and studied the spectra produced by the accretion disk surrounding the central object in the assumption that the baryonic matter in the disk does not interact with the dark matter particles in the envelope.

Under a series of assumptions for the dark matter component of the system, namely

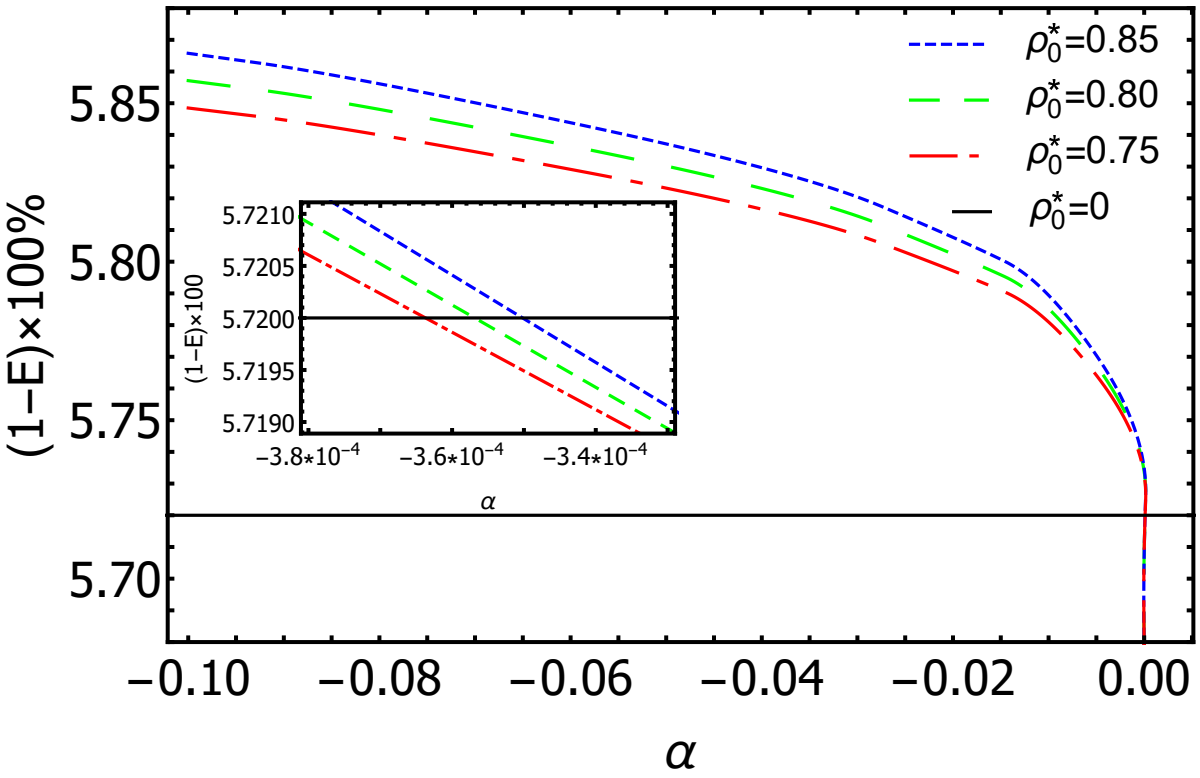

Figure 8.6: Efficiency $\eta = (1 - E(r_{ISCO})) \times 100\%$ versus α. Black solid line corresponds to the efficiency of the Schwarzschild black hole. Color curves shows efficiency in the presence of dark matter with different densities.

density profile, anisotropies and inner boundary, we solved the TOV equations to determine the geometry inside the dark matter envelope and consequently the motion of test particles within the disk. We then numerically evaluated the flux and luminosity of the disk in the presence of dark matter and compared it with the isotropic case and the vacuum case.

We showed that there exist frequencies in the spectrum of accretion disk that bear the mark of the presence of dark matter and that are also affected by the anisotropies. This suggests that if other relevant quantities, such as the mass of the central black hole and the innermost stable circular orbit, can be determined independently, it could be possible, at least in principle, to distinguish different cases. In addition, we also estimated how the radiative efficiency of the source is affected by the presence of dark matter anisotropies and found that the efficiency increases with respect to that of a Schwarzschild black hole immersed in isotropic dark matter when $P_\theta < P$.

Of course, the scenario presented here is just a simple toy model to highlight the qualitative features that the presence of anisotropies may bear on the accretion disk's spectrum. Astrophysical black holes are expected to be rotating and, therefore, the assumption of staticity, while simplifying the equations, is not particularly realistic. However, we expect similar results to hold in the presence of rotation of the central object and we aim at investigating those in future works.

At present, our knowledge of the dark matter distribution near the center of galaxies is very limited, with most studies providing estimates for the dark matter density at distances of the order of several parsecs from the galactic center in the Milky Way. Similar estimates for other galaxies are missing. Similarly, we still don't know whether the geometry near compact objects at the center of galaxies is well described by the Kerr metric. We showed here that the presence of dark matter may affect the spectrum of the black hole's accretion disk and, therefore, provide valuable information on the nature of dark matter itself. The hope is that future observations will allow to test such ideas and further constrain the properties of viable dark matter candidates.

Table 8.1: Physical parameters of the dark matter envelope with fixed $\rho_0 = 0.85 \times 10^{-5} AU^{-2}$ and $P_b = 2.356 \times 10^{-8} AU^{-2}$. In addition the black hole mass $M_{BH} = 5 \times 10^8 M_\odot \approx 4.933 AU$, the corresponding gravitational radius $r_g = 2M_{BH}$, the inner edge of the dark matter envelope $r_b = 5.5 M_{BH}$ are the model free parameters and therefore are also fixed. The choice of the anisotropic parameter α determines the innermost stable circular orbit radius r_{ISCO}, the radius of the dark matter envelope r_s and its total mass $M_{DM}(r_s)$. First column shows various values of α, second r_{ISCO} in units of the gravitational radius r_T corresponding to the total mass of the system $M_T = r_T/2$, third r_s in units of r_T, fourth $M_{DM}(r_s)$ in units of M_T, fifth M_T in units of solar mass and sixth the radiative efficiency of the source $\eta = (1 - E(r_{ISCO})) \times 100\%$.

α	r_{ISCO} (r_T)	r_s (r_T)	$10^{-2} M_{DM}(r_s)$ (M_T)	M_T $(10^8 M_\odot)$	η (%)
-0.10	2.928	5.750	1.7761957	5.0904157	5.866
-0.08	2.925	5.912	1.8099900	5.0921677	5.856
-0.06	2.921	6.124	1.8488401	5.0941833	5.845
-0.04	2.916	6.427	1.8954049	5.0966012	5.830
-0.02	2.909	6.957	1.9561495	5.0997589	5.808
-0.01	2.903	7.498	1.9982066	5.1019474	5.789
-10^{-3}	2.891	9.359	2.0609501	5.1052160	5.747
-10^{-5}	2.882	13.268	2.0786001	5.1061361	5.706
-10^{-7}	2.879	17.343	2.0792547	5.1061703	5.686
-10^{-9}	2.876	21.534	2.0792725	5.1061712	5.674
0	2.875	24.086	2.0792729	5.1061712	5.670
6.78×10^{-11}	2.874	28.626	2.0792729	5.1061712	5.664
6.85×10^{-11}	2.874	29.726	2.0792730	5.1061712	5.662
6.887×10^{-11}	2.872	39.936	2.0792730	5.1061712	5.655

Table 8.2: The intersection points between several luminosity curves with $\rho_0 = 0.85 \times 10^{-5} AU^{-2}$ and $P_b = 2.356 \times 10^{-8} AU^{-2}$ and different values of α and the luminosity curve of a Schwarzschild black hole in vacuum $\rho_0 = 0$. First column shows the different values of α considered, the second and third columns show the frequencies of the emitted radiation and the spectral luminosity as for Fig. 8.5.

α	$\log_{10}(h\nu/kT_*)$	$\log_{10}(\nu\mathcal{L}_{\nu,\infty})$
-9×10^{-9}	-0.603	-1.764
-10^{-9}	-0.651	-1.670
0	-0.756	-1.606
6.78×10^{-11}	-12.254	-33.397
6.85×10^{-11}	-14.683	-39.156

Bibliography

[1] Medeu Abishev, Nurzada Beissen, Farida Belissarova, Kuantay Boshkayev, Aizhan Mansurova, Aray Muratkhan, Hernando Quevedo, and Saken Toktarbay.
Approximate perfect fluid solutions with quadrupole moment.
International Journal of Modern Physics D, 30(13):2150096, 2021.

[2] A. Allahyari, H. Firouzjahi, and B. Mashhoon.
Quasinormal modes of a black hole with quadrupole moment. Phys. Rev. D 99, 044005, 2018.

[3] Armando Bernui and Edwin Portocarrero.
Study of the matching of solutions of the einstein equations according to darmois.
The Astrophysical Journal, 427:947–950, 1994.

[4] Donato Bini, Andrea Geralico, Orlando Luongo, and Hernando Quevedo.
Generalized kerr spacetime with an arbitrary mass quadrupole moment: geometric properties versus particle motion.
Classical and Quantum Gravity, 26(22):225006, 2009.

[5] Kuantay Boshkayev, Hernando Quevedo, Saken Toktarbay, Bakytzhan Zhami, and Medeu Abishev.
On the equivalence of approximate stationary axially symmetric solutions of the Einstein field equations.
Grav. Cosmol., 22(4):305–311, 2016.

[6] Jerónimo Cortez, Dario Núñez, and Hernando Quevedo.
Gravitational fields and nonlinear σ-models.
International Journal of Theoretical Physics, 40(1):251–260, 2001.

[7] Georges Darmois.
Les équations de la gravitation einsteinienne, volume 25.
Gauthier-Villars Paris, 1927.

[8] F. de Felice.
Repulsive gravity and curvature invariants in general relativity.
Annales de Physique Colloque Supplement, 14:79–83, December 1989.

[9] MSR Delgaty and Kayll Lake.
Physical acceptability of isolated, static, spherically symmetric, perfect fluid solutions of einstein's equations.
Computer Physics Communications, 115(2-3):395–415, 1998.

[10] G Erez and N Rosen.
The gravitational field of a particle possessing a multipole moment.
Technical report, Israel Inst. of Tech., Haifa, 1959.

[11] Frederick J Ernst.
New formulation of the axially symmetric gravitational field problem. ii.
Physical Review, 168(5):1415, 1968.

[12] Francisco Frutos-Alfaro, Hernando Quevedo, and Pedro A Sanchez.
Comparison of vacuum static quadrupolar metrics.
Royal Society open science, 5(5):170826, 2018.

[13] Robert Geroch.
Multipole moments. ii. curved space.
Journal of Mathematical Physics, 11(8):2580–2588, 1970.

[14] Roberto Giambò, Orlando Luongo, and Hernando Quevedo.
Repulsive regions in lemaître–tolman–bondi gravitational collapse.
Physics of the Dark Universe, 30:100721, 2020.

[15] Eric Gourgoulhon.
3+ 1 formalism and bases of numerical relativity.
arXiv preprint gr-qc/0703035, 2007.

[16] Antonio C Gutiérrez-Piñeres and Hernando Quevedo.
C3 matching for asymptotically flat spacetimes.
Classical and Quantum Gravity, 36(13):135003, 2019.

[17] Richard O Hansen.
Multipole moments of stationary space-times.
Journal of Mathematical Physics, 15(1):46–52, 1974.

[18] B Kent Harrison.
New solutions of the einstein-maxwell equations from old.
Journal of Mathematical Physics, 9(11):1744–1752, 1968.

[19] Francisco J Hernández, Francisco Nettel, and Hernando Quevedo.
Gravitational fields as generalized string models.
Gravitation and Cosmology, 15(2):109–120, 2009.

[20] L. Herrera, J. Martin, and J. Ospino.
Anisotropic geodesic fluid spheres in general relativity.
Journal of Mathematical Physics, 43(10):4889–4897, October 2002.

[21] Markus Heusler.
Black hole uniqueness theorems.
Cambridge University Press, 1996.

[22] Cornelius Hoenselaers and Werner Dietz.
Solutions of einstein's equations: techniques and results.
Solutions of Einstein's Equations: Techniques and Results, 205, 1984.

[23] Werner Israel.
Singular hypersurfaces and thin shells in general relativity.
Il Nuovo Cimento B (1965-1970), 44(1):1–14, 1966.

[24] Roy P Kerr.
Gravitational field of a spinning mass as an example of algebraically special metrics.
Physical review letters, 11(5):237, 1963.

[25] Kayll Lake.
Revisiting the darmois and lichnerowicz junction conditions.
General Relativity and Gravitation, 49(10):1–11, 2017.

[26] Thomas Lewis.
Some special solutions of the equations of axially symmetric gravitational fields.
Proceedings of the Royal Society of London. Series A, Containing Papers of a Mathematical and Physical Character, 136(829):176–192, 1932.

[27] André Lichnerowicz.
Théorie globale des connexions et des groupes d'holonomie.
Roma 1955, 1955.

[28] Orlando Luongo and Hernando Quevedo.
Toward an invariant definition of repulsive gravity.
In *The Twelfth Marcel Grossmann Meeting: On Recent Developments in Theoretical and Experimental General Relativity, Astrophysics and Relativistic Field Theories (In 3 Volumes)*, pages 1029–1031. World Scientific, 2012.

[29] Orlando Luongo and Hernando Quevedo.
Characterizing repulsive gravity with curvature eigenvalues.
Physical Review D, 90(8):084032, 2014.

[30] Orlando Luongo and Hernando Quevedo.
Characterizing repulsive gravity with curvature eigenvalues.
Physical Review D, 90(8):084032, 2014.

[31] Orlando Luongo and Hernando Quevedo.
Self-accelerated universe induced by repulsive effects as an alternative to dark energy and modified gravities.
Foundations of Physics, 48(1):17–26, 2018.

[32] Daniele Malafarina, Giulio Magli, and Luis Herrera.
Static axially symmetric sources of the gravitational field.
In *AIP Conference Proceedings*, volume 751, pages 185–187. American Institute of Physics, 2005.

[33] Charles W Misner.
Harmonic maps as models for physical theories.
Physical Review D, 18(12):4510, 1978.

[34] Charles W. Misner, K. S. Thorne, and J. A. Wheeler.
Gravitation.
W. H. Freeman, San Francisco, 1973.

[35] I. D. Novikov and K. S. Thorne.
Astrophysics of black holes.
In *Black Holes (Les Astres Occlus)*, page 343, Jan 1973.

[36] Achille Papapetrou.
Eine rotationssymmetrische lösung in der allgemeinen relativitätstheorie.
Annalen der Physik, 447(4-6):309–315, 1953.

[37] Joseph Polchinski.
String theory.
2005.

[38] D. Pugliese, H. Quevedo, and R. Ruffini.
Circular motion of neutral test particles in Reissner-Nordström spacetime.
Phys. Rev. D, 83:024021, 2011.

[39] Daniela Pugliese, Hernando Quevedo, and Remo Ruffini.
Circular motion of neutral test particles in Reissner-Nordström spacetime.
Physical Review D, 83(2):024021, January 2011.

[40] Hernando Quevedo.
General static axisymmetric solution of einstein's vacuum field equations in prolate spheroidal coordinates.
Physical Review D, 39(10):2904, 1989.

[41] Hernando Quevedo.
Generating solutions of the einstein-maxwell equations with prescribed physical properties.
Physical Review D, 45(4):1174, 1992.

[42] Hernando Quevedo.
Mass Quadrupole as a Source of Naked Singularities.
International Journal of Modern Physics D, 20(10):1779–1787, 2011.

[43] Hernando Quevedo.
Matching conditions in relativistic astrophysics.
In *The Twelfth Marcel Grossmann Meeting: On Recent Developments in Theoretical and Experimental General Relativity, Astrophysics and Relativistic Field Theories (In 3 Volumes)*, pages 35–52. World Scientific, 2012.

[44] Hernando Quevedo and Bahram Mashhoon.
Exterior gravitational field of a rotating deformed mass.
Physics Letters A, 109(1-2):13–18, 1985.

[45] H. Stephani, D. Kramer, M. MacCallum, C. Hoenselaers, and E. Herlt.
Exact solutions of Einstein's field equations.
Cambridge University Press, 2003.

[46] Hans Stephani, Dietrich Kramer, Malcolm MacCallum, Cornelius Hoenselaers, and Eduard Herlt.
Exact solutions of Einstein's field equations.
Cambridge university press, 2009.

[47] BH Voorhees.
Static axially symmetric gravitational fields.
Physical Review D, 2(10):2119, 1970.

[48] Hermann Weyl.
Zur gravitationstheorie.
Annalen der Physik, 359(18):117–145, 1917.

[49] VA Belinski VE Zakharov.
Integration of the einstein equation by means of the inverse scattering problem technique and construction of exact solitons solutions.
Journal of experimental e theoretical physics, 48, 1978.

[50] David M Zipoy.
Topology of some spheroidal metrics.
Journal of Mathematical Physics, 7(6):1137–1143, 1966.